https://doi.org/10.5194/wes-2025-57
Preprint. Discussion started: 8 April 2025
© Author(s) 2025. CC BY 4.0 License.

WIND ENERGY SCIENCE DISCUSSIONS
Open Access

Wind dataset assessment and energy estimation for potential future offshore wind farm development areas on the Scotian Shelf

Yongxing Ma[1], Jinshan Xu[1], Yongsheng Wu[1], Michael Z. Li[2], Ryan Stanley[1], Brent Law[1], and Marc Skinner[1]

[1]Fisheries and Oceans Canada, Bedford Institute of Oceanography, 1 Challenger Drive, Dartmouth, B2Y 4A2, Nova Scotia, Canada
[2]Geological Survey of Canada (Atlantic), Bedford Institute of Oceanography, 1 Challenger Drive, Dartmouth, B2Y 4A2, Nova Scotia, Canada

Correspondence: Yongxing Ma (Yongxing.Ma@dfo-mpo.gc.ca) and Yongsheng Wu (Yongsheng.Wu@dfo-mpo.gc.ca)

Abstract. The Scotian Shelf is one of the top wind regimes in the world. In order to assess the wind energy of the potential wind farms over the shelf, in this study, we first assessed the uncertainties of four commonly used wind datasets: ERA5, CFSv2, NARR, and HRDPS, by comparing them against observational wind data distributed at both nearshore and offshore sites. The assessment indicates that the root-mean-square error of the datasets varies between 1.6 m/s and 2.4 m/s in wind speed and between 24.6° and 36.4° in wind direction. HRDPS performs better at the near-shore sites, while ERA5 is more accurate at the offshore sites. We then estimated the wind energy potential of six wind farms on the shelf using ERA5 and HRDPS. The estimation shows that wind energy varies seasonally, the energy in summer 55% lower than that in winter. The uncertainties in wind datasets enhance the variation of the wind energy production, up to 28% in winter and 55% in summer. The energy output is sensitive to turbine spacing due to wind wakes, which reduce energy by 17% to 26% in winter and by 40% to 55% in summer, depending on the relationships between wind speeds, wind directions, and the specific layout of the wind farms. This strong variation in wind energy output suggests that a more feasible operational method should be used to balance energy production and usage.

1 Introduction

1.1 Background

Offshore wind farms have rapidly developed globally over the past decade (World Forum Offshore Wind, 2024), driven in part by greater consistency and abundance of wind resources compared to onshore. By the end of 2023, the capacity in operation of global offshore wind farms had reached 67.4 GW, and is projected to reach 414 GW by 2032, which is a significant increase from 7.9 GW in 2014 (World Forum Offshore Wind, 2024). Although no wind turbines have been installed in Canadian offshore waters to date, offshore wind is expected to play a key role in Canada's electricity portfolio in support of the country's net-zero emissions goal by 2050 (Canada Energy Regulator, 2023). Nova Scotia's offshore waters rank among the world's best wind resources, with average wind speeds of 9–11 m/s at 100 metres above the ocean surface (Aegir Insights ApS, 2023; Nicholson,

https://doi.org/10.5194/wes-2025-57
Preprint. Discussion started: 8 April 2025
© Author(s) 2025. CC BY 4.0 License.

2023). The federal and provincial governments plan to offer leases for 5 GW of offshore wind development on the Scotian Shelf by 2030 (Government of Nova Scotia, 2023).

As planning for offshore wind development on the Scotian Shelf progresses, there remains a lack of comprehensive assessments of wind datasets and, particularly, estimates of wind energy potential that accounts for wake effects associated with varying wind turbine spacing. To address this gap, this study evaluated available wind datasets, comparing their accuracy against regional wind observations to better inform the region's offshore wind potential. These datasets were then used to simulate wind farm performance across potential future development areas (PFDAs), incorporating turbine spacing and wake effects to assess their influence on energy production. While the PFDAs analyzed in this study generally align with proposed offshore wind energy areas for the Scotian Shelf, their exact location, shape, and size may differ from final areas that are approved for development.

This research aimed to provide a more accurate estimate of wind energy potential on the Scotian Shelf, as well as offer insight into future wind farm planning, design, and development in the region. The manuscript is structured as follows: Section 2 introduces the wind datasets, regional wind observations, and metrics used for evaluation, along with the PyWake model configuration; Section 3 presents the wind dataset assessment results for wind speed and wind direction; Section 4 presents PFDAs power production simulation results; and finally, Sections 5 and 6 present discussions and conclusions, respectively.

1.2 Wind Datasets

Offshore wind development on the Scotian Shelf requires reliable wind resource assessments to guide investment and planning, particularly as this industry is new to the region. Previous studies evaluating potential power generation for the PFDAs on the Scotian Shelf have relied on climatological wind speeds and idealized conditions (i.e., Aegir Insights ApS (2023); Kilpatrick et al. (2023)). However, these studies did not account for turbine wake effects, which can significantly influence overall energy potential and lead to inaccurate energy estimates. A more robust approach involves simulating offshore wind farms using numerical models that incorporate time-varying wind speed and wind direction data from wind datasets, providing a more accurate foundation for decision-making.

There are several reanalysis and forecast wind datasets that cover the Scotian Shelf region, including: 1) the fifth-generation European Centre for Medium-Range Weather Forecasts (ECMWF) atmospheric reanalysis (ERA5); 2) Climate Forecast System Version 2 (CFSv2); 3) North American Regional Reanalysis (NARR); and 4) High-Resolution Deterministic Prediction System (HRDPS). Assessments of wind speed from these datasets have been carried out for other regions (e.g., Fan et al., 2021; Gualtieri, 2021; Kardakaris et al., 2021; Wang et al., 2019). Although these assessments have had varied objectives, such as dataset evaluation (Milbrandt et al., 2016), inter-dataset comparison (Wang et al., 2019; Fan et al., 2021), and wind energy estimations (Li et al., 2010; Murcia et al., 2022), they all strengthened our understanding of global different datasets and provided guidance in selecting the most suitable dataset for specific applications.

To assess the ability of available wind datasets to reflect conditions on the Scotian Shelf, this study compared the wind speed against observational wind measurements using statistical metrics including Root Mean Square Error (RMSE), bias, Mean Absolute Error (MAE), and the correlation coefficient or coefficient of determination (R^2) (Gualtieri, 2021; Fan et al., 2021;

https://doi.org/10.5194/wes-2025-57
Preprint. Discussion started: 8 April 2025
© Author(s) 2025. CC BY 4.0 License.

Open Access WIND ENERGY SCIENCE DISCUSSIONS

Kardakaris et al., 2021; Wang et al., 2019; Milbrandt et al., 2016; Murcia et al., 2022). To align gridded wind datasets with the more limited observational data, horizontal interpolation using a 2-D linear or cubic methods, and vertical extrapolations using a power law relationship, assuming atmospheric neutral stability (Wang et al., 2019; Kardakaris et al., 2021; Murcia et al., 2022), can be used.

Among the four wind datasets, ERA5 has been the most widely assessed and often deemed to be one of the most accurate. Fan et al. (2021) evaluated five wind datasets (i.e., ERA5, ERA-Interim, JRA-55, MERRA-2, and CFSv2) by comparing 10-m wind speed data to wind observations from over 1000 meteorological stations worldwide. The authors found that ERA5 demonstrated the best overall performance among the five reanalysis wind dataset products, with ERA5 exhibiting a mean percent bias for all stations of -4.54%, while the mean percent bias ranged from -54.22% for JRA-55 and 42% for MERRA-2. Similarly, in a recent dataset validation study, Murcia et al. (2022) compared multiple wind datasets with wind observations from various sites across Europe and found that after calibration, ERA5 outperformed all other datasets, including the European-level atmospheric reanalysis (EIWR). In general, the ERA5 dataset exhibited the lowest MAE, smallest RMSE, and highest correlation coefficient.

Gualtieri (2021) compared ERA5 wind speeds against wind measurements taken from six tall towers spread across a diverse range of global locations. This comparison noted that the normalized bias of wind speed ranged from -0.18 to 0.53, while the correlation coefficient between ERA5 and wind observations varied from 0.38 to 0.96, depending on location. Similar findings were reported by Fan et al. (2021), whose results indicated notable regional differences, with the percent bias for ERA5 ranging from -11.55% in Australia to 16.13% in Central Asia.

Even within a relatively small region, wind dataset reanalysis products can exhibit considerable spatial variability. For example, Kardakaris et al. (2021) assessed ERA5 wind speed using measurements from six buoys in the Greek seas and found that the relative difference between ERA5 and observed wind speeds ranged from 6.5% to 34.7%. Similarly, Fernandes et al. (2021) compared ERA5 wind speed data at the height of 100 m above sea surface with wind observations from both coastal and offshore sites in Brazil. The findings showed that in the coastal region the bias was less than 0.5 m/s (with a mean wind speed of approximately 6 m/s), whereas in the offshore region the bias was nearly zero (with a mean wind speed of 7.19 m/s).

Li et al. (2010) compared 80-m-height wind speed observations from rawinsondes in the Great Lakes region of the United States to the NARR wind dataset. Their analysis showed that the bias ranged from -0.64 m/s to 0.59 m/s, exhibiting a characteristic wind speed of 6 m/s and a correlation coefficient close to 0.8, suggesting that NARR provided an accurate simulation of wind speed for the study region. Further, Wang et al. (2019) assessed the 10-m wind speed and wind direction from various datasets, including NARR, against wind observations from three ocean buoys along the Central California Coast. The authors found that the NARR dataset generally underestimated wind speed compared to observations from all three buoys, with the bias ranging from -2.78 m/s to -0.15 m/s and RMSE from 1.90 m/s to 4.00 m/s for mean wind speeds between 4 m/s and 11 m/s.

There are limited studies that have evaluated the HRDPS dataset to observed wind speeds (e.g., Milbrandt et al., 2016; Moore-Maley and Allen, 2022). Notably, in a nearshore area, Moore-Maley and Allen (2022) examined 5-year hourly surface wind speed records against wind observations from four stations (meteorological stations and ocean buoys) in the Salish Sea.

https://doi.org/10.5194/wes-2025-57
Preprint. Discussion started: 8 April 2025
© Author(s) 2025. CC BY 4.0 License.

The authors observed an overall qualitative consistency between HRDPS and the observations in terms of wind speed and wind direction.

In general, most wind dataset assessment studies have focused on the evaluation of wind speed, with fewer studies assessing wind direction (Moore-Maley and Allen, 2022). Assessing wind direction, however, is important for the purpose of conducting wind farm simulations, as wind direction and turbine layout can influence wind farm efficiency due to wake effects (Gaumond et al., 2014; Stieren et al., 2021).

1.3 Wake Effects

In general, studies that have estimated offshore wind farm energy potential from wind datasets (e.g., Wang et al., 2022; Gualtieri, 2021; Kardakaris et al., 2021; Fernandes et al., 2021) typically estimate wind power using simple formulas or interpolate using wind turbine power curves. However, these approaches can overlook a key aspect of real-world conditions; primarily, wind turbines can generate wake effects that reduce wind speeds available to downstream turbines, leading to lower overall energy production from a wind farm. Wake effects have been estimated to result in energy losses on order of 10% to 25% in medium-sized offshore wind farms, such as the Horns Rev, Lillgrund, and Nysted wind farms (Barthelmie et al., 2009, 2010; Niayifar and Porté-Agel, 2015; Simisiroglou et al., 2019; Wu and Porté-Agel, 2015). For large-sized offshore wind farms, Pryor et al. (2021) estimated, through simulation, an overall 35.3% energy loss associated with wake effects.

Given the impact wake effects can have on wind farm efficiency, substantial research has been dedicated to predicting turbine wakes using analytical models (e.g., Bastankhah and Porté-Agel, 2014; Jensen, 1983; Niayifar and Porté-Agel, 2015), numerical simulations (e.g., Calaf et al., 2010; Pryor et al., 2021; Stevens, 2016; Troldborg et al., 2010), and laboratory experiments (e.g., Chamorro and Porté-Agel, 2010). In recent studies (e.g., Fischereit et al., 2022; Murcia et al., 2022), wake effects were incorporated into wind farm energy production estimates using PyWake (Pedersen et al., 2023), which is a Python package designed to efficiently calculate wake interactions in wind farms.

In addition to wake effect models, wind farm simulations also require detailed turbine models and turbine layouts. Older offshore wind farms deployed smaller turbines; for example, the Horns Rev wind farm utilized Vestas V80 2 MW turbines (Hansen et al., 2012). In contrast, Siemens 2.3 MW turbines were installed at Nysted and Lillgrund (Barthelmie et al., 2010; Simisiroglou et al., 2019). More recently, there has been a move towards installation of larger turbines. The average rated-capacity of installed offshore wind turbines globally has been increasing, with an average of 4.0 MW in 2013, 9.7 MW in 2023, and a projected increase to 14.8 MW by 2028 (McCoy et al., 2024). In the U.S., several offshore wind farms currently under construction are now incorporating 15 MW turbines (Tetra Tech Inc., 2022).

Turbine spacing is a critical factor that influences wake effect energy losses in a wind farm. Larger turbine spacing allows downstream wind more space to regain velocity through turbulent mixing, which draws kinetic energy downward from higher atmospheric layers (Frandsen, 1992). This larger spacing thus can improve the efficiency of downstream wind turbines, compared to those spaced closer together. However, increased spacing can also lead to overall reduced energy generation given fewer turbines being emplaced within a development area. These factors emphasize the importance of understanding the trade-offs between turbine spacing and wake effects, in an effort to inform overall economics of wind farm planning, design, and

https://doi.org/10.5194/wes-2025-57
Preprint. Discussion started: 8 April 2025
© Author(s) 2025. CC BY 4.0 License.

development (Mulas Hernando et al., 2023; Stevens et al., 2017). Typical turbine spacing ranges from 4 to 11 D, where D is the turbine rotor diameter (Bosch et al., 2019; Pryor et al., 2021; Stevens et al., 2017). At the Lillgrund offshore wind farm in Sweden, turbine spacing ranges 3.3 to 4.3 D (Simisiroglou et al., 2019), while at the Horns Rev offshore wind farm in Denmark the turbines are spaced at 7 D (Barthelmie et al., 2010).

2 Datasets and Methods

2.1 Regional Wind Observations

Hourly wind data from weather stations within the Scotian Shelf area were obtained from the Government of Canada's Historical Climate Data website (https://climate.weather.gc.ca). Two island-based meteorological stations located at a nearshore site (Beaver Island) and an offshore site (Sable Island) on the Scotian Shelf were selected for analysis. For the oceanic domain, wind data were obtained from moored marine buoy sites. Four buoys were selected based on data coverage for the analysis period and minimal gaps in observed wind data (Figure 1). These data were obtained from the Fisheries and Oceans Canada (DFO) Marine Environmental Data Section Archive (https://meds-sdmm.dfo-mpo.gc.ca). All sites were summarized in Table 1. The sites were numbered in a sequence based on distance away from the coastline of Nova Scotia and in a northeast to southwest direction. Due to different regimes of wind dynamics (Cañadillas et al., 2023; Djath et al., 2022), the sites have been categorized as nearshore (Sites 1 and 2) and offshore (Sites 3–6).

Table 1. Information on the meteorological stations and marine buoy sites used in this study. For meteorological stations, the height corresponds to the station's elevation above sea level, with wind measurements taken by an anemometer mounted on a mast at a height of 10 meters above the ground. For marine buoys, the listed height represents the height of the instrument measuring winds above the sea surface.

Site	Longitude (°W)	Latitude (°N)	Height (m)	Group	Type
1	62.33	44.82	16.0	nearshore	meteorological station
2	63.40	44.50	5.0	nearshore	marine buoy
3	59.96	43.93	1.2	offshore	meteorological station
4	64.02	42.51	5.0	offshore	marine buoy
5	57.10	44.24	5.0	offshore	marine buoy
6	62.00	42.26	5.0	offshore	marine buoy

2.2 Wind Datasets

The ERA5 dataset, developed by ECMWF, is a reanalysis climate product that assimilates historical observational data globally (Hersbach et al., 2020). It has global coverage with spatial resolution of 0.25° and spans from January 1940 to the present with hourly frequency. The 10-m wind velocity components in east-west and north-south directions can be accessed at the Copernicus Climate Data Store (Hersbach et al., 2023).

https://doi.org/10.5194/wes-2025-57
Preprint. Discussion started: 8 April 2025
© Author(s) 2025. CC BY 4.0 License.

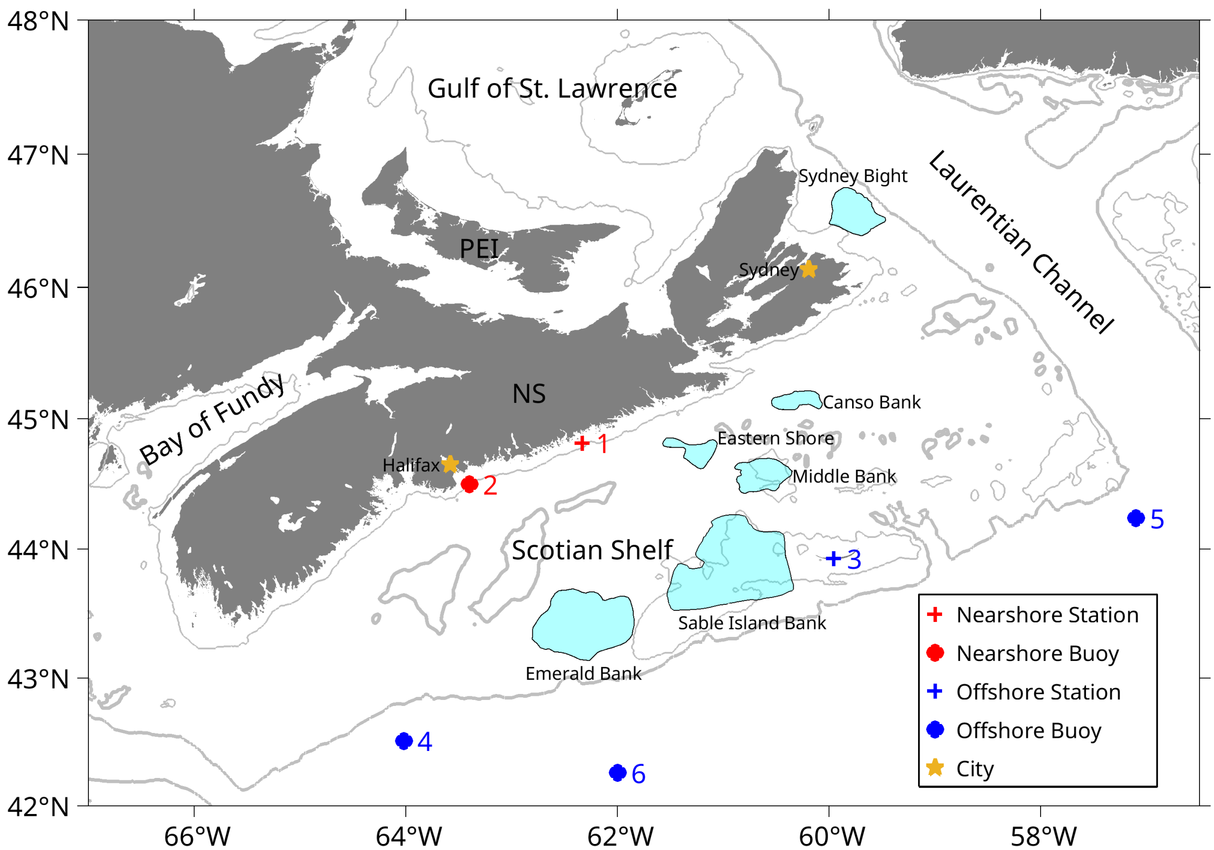

Figure 1. Map of the Scotian Shelf study area located in the offshore of Nova Scotia, Atlantic Canada. The map illustrates locations of regional wind observation sites, including meteorological stations (+) and marine buoys (•) at both nearshore (red) and offshore (blue) locations. The potential future development areas (PFDAs) for offshore wind farms used in this study are also named. These PFDAs are adapted from general areas described by Committee for the Regional Assessment of Offshore Wind Development in Nova Scotia (2024). Although the PFDAs used in this study generally align with offshore wind energy areas being discussed for the Scotian Shelf, the exact areas used in this study may differ in location, shape, and size from those areas finalized by regulators for offshore wind development consideration. Cities are illustrated with yellow stars. Contour lines at 100-m and 200-m isobaths are depicted with thin and thick grey curves, respectively. NS = Province of Nova Scotia; PEI = Province of Prince Edward Island.

The CFSv2 is a coupled model that contains ocean, land, and atmosphere components (Saha et al., 2014). The National Centers for Environmental Prediction (NCEP) provides selected hourly time-series products of CFSv2 dataset that span from April 1, 2011, to the present. Hourly time series of 10-m wind velocity components in two directions, with a 0.2° horizontal resolution, can be accessed from the Research Data Archive at the National Center for Atmospheric Research (Saha et al., 2011).

The NARR dataset produced by NCEP provides a high-resolution reanalysis of atmospheric variables, including wind velocities (Mesinger et al., 2006). The 3-hourly wind velocity at 10 m height can be acquired from the Research Data Archive

https://doi.org/10.5194/wes-2025-57
Preprint. Discussion started: 8 April 2025
© Author(s) 2025. CC BY 4.0 License.

at the National Center for Atmospheric Research (National Centers for Environmental Prediction, National Weather Service, NOAA, U.S. Department of Commerce, 2005).

The HRDPS developed by Environment and Climate Change Canada (ECCC) is a high-resolution numerical weather prediction model with assimilation (Milbrandt et al., 2016). It has a spatial resolution of 2.5 km and an hourly temporal frequency. The dataset spans from April 23, 2015, to the present, covering all of Canada. Information on accessing the HRDPS dataset can be found at the Meteorological Service of Canada Open Data portal (https://eccc-msc.github.io/open-data/msc-data/readme_en/). Table 2 summarizes the basic parameters associated with all four wind datasets.

Table 2. Summary information for the four wind datasets used in this study: ERA5, CFSv2, NARR, and HRDPS.

Name	Source	Time Range	Horizontal Resolution	Temporal Resolution	Spatial Coverage
ERA5	ECMWF	1940–present	0.25°	hourly	Global
CFSv2	NCEP	2011–present	0.2°	hourly	Global
NARR	NCEP	1979–present	0.3°	3-hourly	North America
HRDPS	ECCC	2015–present	2.5 km	hourly	Canada (mainly)

2.3 Spatial and Temporal Interpolation

Since the wind datasets and regional wind observations do not align in space or time the respective coordinates were standardized. To do this, a 2-D linear interpolation was applied to the gridded wind datasets to match the wind observation site locations. Since the wind datasets provided velocity components along the east-west and north-south directions, separate interpolations for each of the components were performed. The ERA5, CFSv2, and HRDPS wind datasets have identical time intervals, corresponding to exact hours. In contrast, the NARR dataset is provided at 3-hour intervals (i.e., 00:00, 03:00, 06:00, ..., 21:00).

To align the NARR data with ERA5 time intervals, another 1-D linear interpolation was performed along the time dimension. Although the wind observation times were approximately one hour apart, they did not align exactly with the hour marks. To enable comparison between the two wind datasets, the observation times were interpolated to match the hourly timestamps of the ERA5 dataset. Since the observation data were in the form of wind speed and wind direction, a straightforward linear interpolation for wind speed was applied. For wind direction, the interpolation method for angular values described by Berens (2009) was used.

2.4 Extrapolating Wind Speed

Wind measurements from marine buoys were taken at a height of 5 metres above sea surface, while data from the four wind datasets were taken at 10 metres above the sea surface. To compare data at the same height, the power-law relationship in (1) was applied, assuming a naturally-stable atmospheric condition, to extrapolate wind speed from m to m. The exponent α was

https://doi.org/10.5194/wes-2025-57
Preprint. Discussion started: 8 April 2025
© Author(s) 2025. CC BY 4.0 License.

set to 1/7, which is a common value used in other studies (Fan et al., 2021; Holt and Wang, 2012; Tian et al., 2019; Wang et al., 2016).

$$\frac{U_2}{U_1} = \left(\frac{z_2}{z_1}\right)^{\alpha}. \tag{1}$$

This approach was also used to convert wind speeds from the ERA5 and HRDPS datasets from 10 metres to an assumed turbine hub height at 150 metres (parameters of the turbine model used in this study was introduced in subsection 2.6 below).

2.5 Assessment Metrics

Four metrics to compare wind speed and wind direction observations (denoted as 'O' in the following equations) with the wind datasets (denoted as 'M' in the following equations) were selected: 1) Root Mean Square Error (RMSE); 2) bias; 3) Mean Absolute Error (MAE); and 4) the coefficient of determination (R^2). The metrics were defined as follows.

RMSE is a measure of the magnitude of error between a wind dataset and the observed wind values (2). It provides an indication of how well wind dataset values align with observed wind data, with lower RMSE values indicating better dataset performance. RMSE is calculated as:

$$\mathrm{RMSE} = \sqrt{\frac{1}{N}\sum_{i=1}^{N}(M_i - O_i)^2}, \tag{2}$$

where N is the total number of data points.

Bias is a measure of the overall deviation between a wind dataset and the observed wind values (3). A positive or negative bias indicates that the dataset overestimates or underestimates the wind observations, respectively. Bias is calculated as:

$$\mathrm{Bias} = \frac{1}{N}\sum_{i=1}^{N}(M_i - O_i). \tag{3}$$

MAE is a measure of the average absolute error between a wind dataset and the observed wind values (4). Given each error influences MAE linearly, this metric is straightforward to interpret. MAE is calculated as:

$$\mathrm{MAE} = \frac{1}{N}\sum_{i=1}^{N}|M_i - O_i|. \tag{4}$$

R^2 is a measure of the degree to which the wind dataset matches the observed wind values (5). Its value ranges from 0, representing the worst prediction, to 1, representing a perfect match. R^2 is calculated as:

$$R^2 = 1 - \frac{\sum_{i=1}^{N}(M_i - O_i)^2}{\sum_{i=1}^{N}(O_i - \bar{O})^2}. \tag{5}$$

Metrics were calculated using wind speeds and wind directions measured at 10-m height above the island surface or sea surface depending on the observation site. Because the study focused on evaluating a wind dataset for wind speed within a turbine's operating range, which is 3 m/s to 25 m/s at the hub height of a 150 m high turbine (Figure 2), the corresponding wind speed range at 10-m height is approximate 2 m/s to 17 m/s based on (1). Therefore, all metrics were only calculated using wind data during periods of wind speed that fell within a range of 2 m/s to 17 m/s.

https://doi.org/10.5194/wes-2025-57
Preprint. Discussion started: 8 April 2025
© Author(s) 2025. CC BY 4.0 License.

2.6 Configuration of Power Production Model For Wind Farm Development Areas

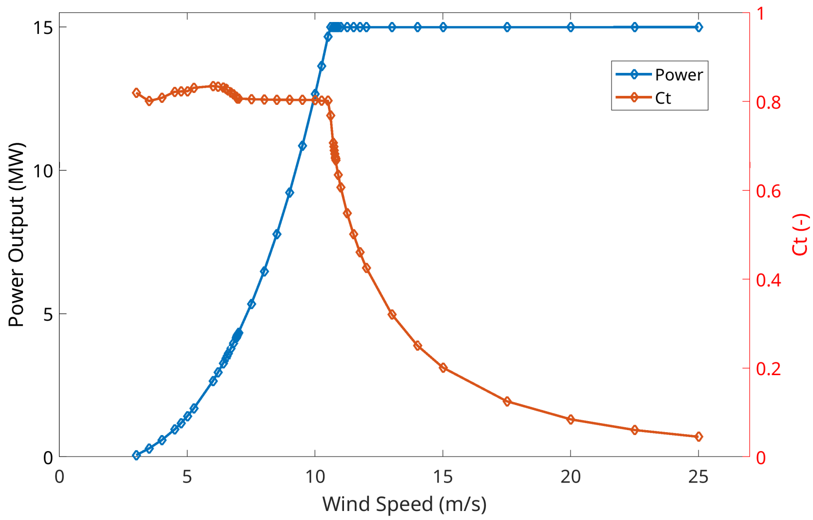

Figure 2. Power curve and thrust coefficient (C_t) versus wind speed used in this study. The turbine model adopted was an IEA 15 MW turbine (Gaertner et al., 2020).

PyWake is a Python package used to simulate wind farm flow fields. It integrates multiple wake models caused by wind turbines and wake interaction models (Pedersen et al., 2023). Validations of PyWake have demonstrated that its results agree well with those from Computational Fluid Dynamic models and observational data (PyWake development team, n.d.; Quick et al., 2024). The turbine model used for simulation in this study was the IEA 15 MW wind turbine (Gaertner et al., 2020). The IEA 15 MW wind turbine features a hub height of 150 metres and the rotor diameter is 240 metres.

The thrust coefficient (C_t) represents the portion of wind energy extracted by the rotor. At lower wind speeds, C_t is high, meaning a larger portion of the wind's energy is extracted for producing electricity, resulting in more pronounced wake effects (Figure 2). As wind speed increases beyond 10.6 m/s (equivalent to 7.2 m/s at 10-m height above surface), C_t decreases, reducing the portion of energy extracted, while the turbine reaches its rated power output of 15 MW. Consequently, wake effects become less pronounced.

In wind farms, turbines located in the interior experience lower wind speeds due to wake effects from upstream turbines. This reduction in wind speed leads to a decrease in power production compared to an ideal scenario with no wake interference. To assess the impact of wakes on turbine performance, the wake efficiency metric was employed in this study, which quantifies how effectively a turbine generates power under wake-influenced conditions. Wake efficiency, η, defined as the ratio of a turbine's actual power output in the presence of wakes, denoted as P_{wake}, to its theoretical power output in an idealized scenario without wake effects, P_{ideal}, is expressed as:

$$\eta = \frac{P_{\text{wake}}}{P_{\text{ideal}}}. \tag{6}$$

https://doi.org/10.5194/wes-2025-57
Preprint. Discussion started: 8 April 2025
© Author(s) 2025. CC BY 4.0 License.

The wake effect was simulated using the wake deficit model of a Gaussian profile type described by Bastankhah and Porté-Agel (2014). The Gaussian-based model is known for its accuracy in describing wake expansion and velocity deficits, especially for modern large-scale turbines. The simulations used hourly wind speed and wind direction sourced from the wind datasets of ERA5 and HRDPS. Since winds on the Scotian Shelf are relatively consistent in space, a spatially-averaged wind speed and wind direction were used in the simulation of each PFDA. This approach simplified simulation setup while also maintaining focus on temporal variability. At a given location, wind speed deficits were often influenced by wake effects from multiple upstream turbines. To account for combined wake effects in this study, the linear superposition sub-model in PyWake was used.

3 Wind Dataset Assessments

3.1 Assessment of Wind Speed

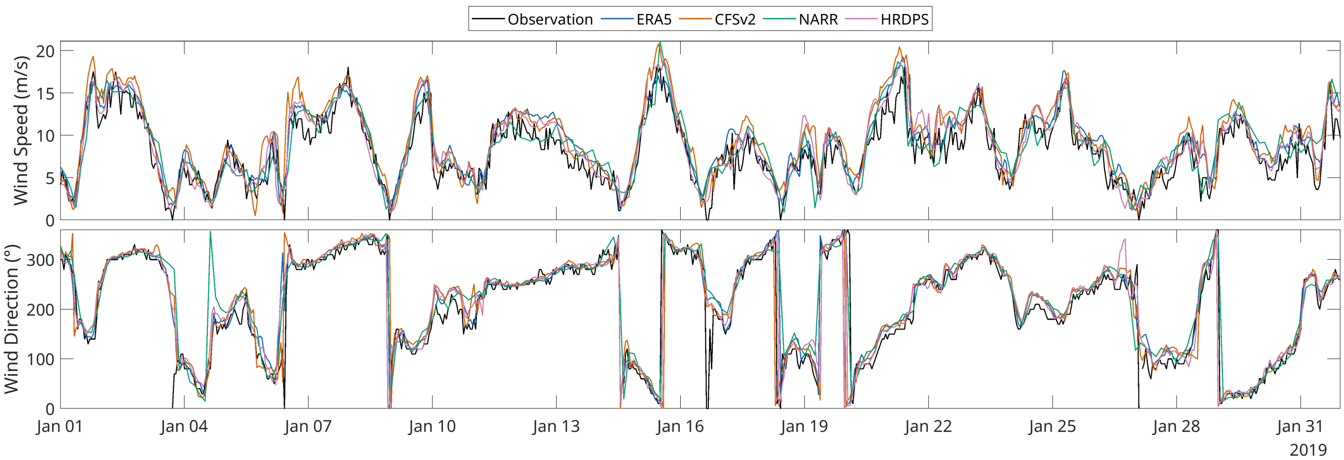

Figure 3. Time series of wind speed (upper panel) and wind direction (lower panel) at Site 3 at a 10-m height above surface for observation and the four wind datasets ERA5, CFSv2, NARR, and HRDPS. The comparison was for the month of January 2019.).

Performance of the wind datasets ERA5, CFSv2, NARR, and HRDPS was assessed by comparing the dataset data with observed wind data using the four metrics described above (Section 2.5). Time series of wind speed and wind direction at a height of 10-m above surface at Site 3, demonstrated general agreement between wind datasets and regional wind observations at the site (Figure 3). All datasets generally captured the variability and magnitude of the observed wind speed at Site 3. However, there were notable discrepancies between the datasets and observations during periods of higher observed wind speeds (e.g., January 6–8, 2019, and January 20–21, 2019), which illustrate that performance of the datasets does vary in time.

In terms of wind direction, the datasets exhibited good agreement with wind observations at Site 3 during most periods of moderate to high wind speeds. In contrast there were larger discrepancies in wind direction during periods of low wind speeds

https://doi.org/10.5194/wes-2025-57
Preprint. Discussion started: 8 April 2025
© Author(s) 2025. CC BY 4.0 License.

(e.g., January 16–17, 2019). In general, the datasets performed well in capturing variations over longer timescales (days to weeks), although they did not consistently capture short-term fluctuations (on a daily scale).

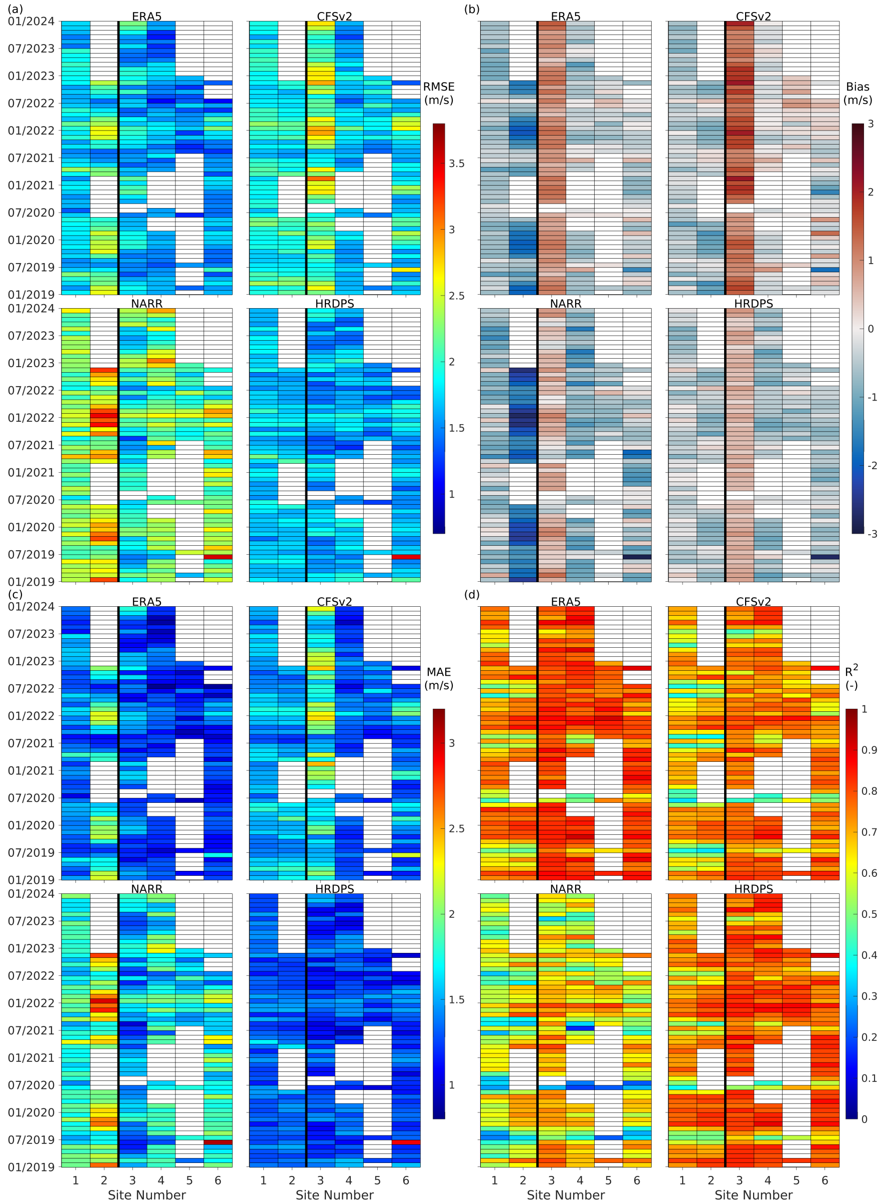

Figure 4. Pseudocolor plots displaying monthly (a) RMSE, (b) bias, (c) MAE, and (d) R^2 for wind speed for each dataset per wind observation site from January 1, 2019, to December 31, 2023. Sites 1 and 2 are representative of the nearshore (left of bold black line in each subplot) and Sites 3 - 6 are representative of the offshore (right of bold black line in each subplot) on the Scotian Shelf. The wind dataset is indicated at the top of each subplot. Blank areas (white pixels) indicate months and sites that had insufficient, valid observation records (considered to be less than 120 observation records in a month). These were considered to be non-valid for purposes of this study.

https://doi.org/10.5194/wes-2025-57
Preprint. Discussion started: 8 April 2025
© Author(s) 2025. CC BY 4.0 License.

To quantitatively evaluate the wind datasets against the wind observations, the four metrics were used, as defined in equations (2)–(5) described above. The four evaluation metrics (RMSE, bias, MAE, and R^2) were calculated on a monthly basis over a five-year period from January 1, 2019 to December 31, 2023, using hourly data pairs of each wind dataset and the wind observations (Figure 4).

At nearshore sites, HRDPS consistently exhibited the lowest RMSE values across most of the months in 2019 – 2023 among the four wind datasets (Figure 4 a). The five-year averaged RMSE values obtained from HRDPS was 1.72 ± 0.15 m/s (mean ± standard deviation calculated from RMSE for all months per observation site) at Site 1 and 1.70 ± 0.13 m/s at Site 2. Following HRDPS, ERA5 displayed higher five-year averaged RMSE values of 1.76 ± 0.20 m/s and 2.08 ± 0.37 m/s at the two corresponding nearshore sites. The CFSv2 dataset exhibited slightly higher five-year averaged RMSE values compared to ERA5, showing values of 1.91 ± 0.17 m/s and 1.92 ± 0.19 m/s at the respective sites. Last, NARR exhibited the highest five-year averaged RMSE values of 2.27 ± 0.21 m/s and 2.69 ± 0.38 m/s at the two respective sites.

At offshore sites, ERA5 exhibited the lowest five-year averaged RMSE values at most sites (i.e., Sites 4, 5 and 6), with the values being 1.54 ± 0.18 m/s, 1.45 ± 0.18 m/s, and 1.58 ± 0.23 m/s, respectively. At Site 3, ERA5 exhibited the second lowest five-year averaged RMSE values across all datasets of 1.72 ± 0.24 m/s, and was only slightly higher than the HRDPS five-year averaged RMSE value of 1.61 ± 0.19 m/s. In contrast, CFSv2 exhibited higher five-year averaged RMSE values compared to ERA5 and HRDPS at all sites. Last, NARR exhibited the highest five-year averaged RMSE values among all datasets; particularly, at Sites 4, 5 and 6 where the NARR monthly RMSE values typically exceeded ERA5 by more than 0.6 m/s.

Seasonal variation in the monthly RMSE values was observed (Figure 4 a), where the RMSE values tended to increase during winter months when wind speeds were higher and decrease in summer months when wind speeds were lower. This seasonal pattern was evident at both nearshore and offshore sites across all four datasets.

For bias at the two nearshore sites (Figure 4 b), HRDPS generally exhibited the smallest deviation from zero among the four datasets. The 5th to 95th percentile range of monthly bias for HRDPS ranged from -0.85 m/s to 0.15 m/s at Site 1 and -0.92 m/s to 0.17 m/s at Site 2. This was followed by CFSv2, which exhibited monthly bias values that ranged from -0.96 m/s to 0.04 m/s at Site 1, and -1.29 m/s to 0.21 m/s at Site 2. ERA5 exhibited a slightly wider range of monthly bias values compared to CFSv2 at both sites; particularly at Site 2 where the monthly bias values for ERA5 were predominantly negative (underestimation). Last, NARR exhibited the widest range of monthly bias among all datasets. Similar to ERA5 at Site 2, the monthly bias for NARR was consistently negative.

For bias at the offshore sites, there was a clear difference between Site 3 (the meteorological station located on Sable Island) and the offshore buoy sites (Sites 4, 5 and 6). At Site 3, the monthly bias was predominantly positive (overestimation) across all four datasets for almost all months. This was likely due to the small size of Sable Island (the island's size approximately 33.5 km east-west and less than 1.5 km north-south), which was believed to be too small to be resolved by the datasets, and consequently, the surface roughness in the numerical models was believed to underestimated. In turn, this would result in overestimated wind speeds within the models.

At the marine buoy Sites 4, 5 and 6, the percentages of monthly bias values from CFSv2 that fell within a range of -0.5 m/s to 0.5 m/s, were 75%, 27%, and 55%, respectively. These values suggested that CFSv2 over-performed the other wind datasets.

https://doi.org/10.5194/wes-2025-57
Preprint. Discussion started: 8 April 2025
© Author(s) 2025. CC BY 4.0 License.

The ERA5 followed with corresponding site percentages of 40%, 23%, and 47% respectively. The HRDPS was the third best performing dataset, with NARR performing the worst, exibiting only 12%, 12%, and 37% of bias values at Sites 4, 5, and 6, respectively, within the -0.5 m/s to 0.5 m/s range. Similar to RMSE, seasonal fluctuations were also evident in bias. At the nearshore sites, bias tended to be more positive during fall months and more negative during spring months. In contrast, bias generally became more negative during fall months and more positive during spring months at the offshore sites.

The monthly MAE over the five-year period was also estimated (Figure 4 c). Similar to the RMSE and bias metrics described above, HRDPS stood out as the best-performing dataset at the two nearshore sites, which exhibited five-year averaged MAE values of 1.33 ± 0.11 m/s and 1.34 ± 0.11 m/s at Sites 1 and 2, respectively. This was followed by ERA5 and CFSv2, which exhibited comparable performance, while NARR exhibited the highest five-year averaged MAE values among all four datasets at both nearshore sites. Offshore, ERA5 exhibited the lowest five-year averaged MAE values of 1.20 ± 0.14 m/s, 1.13 ± 0.14 m/s, and 1.22 ± 0.17 m/s at Sites 4, 5, and 6, respectively. At Site 3, ERA5 exhibited the second lowest five-year averaged MAE of 1.36 ± 0.19 m/s (this followed the lowest five-year averaged MAE value of 1.24 ± 0.14 m/s at Site 3 for HRDPS). Seasonal variation in MAE was similar to those observed for RMSE at the nearshore and offshore sites.

Monthly R^2 (Figure 4 d) exhibited different patterns between the nearshore and offshore sites (Figure 4 d). The R^2 values at nearshore sites were generally lower than those at offshore sites among the four datasets. At nearshore sites, HRDPS exhibited the highest five-year averaged R^2 values of 0.70 ± 0.10, 0.72 ± 0.11 at Sites 1 and 2, respectively. This was followed by ERA5 and then CFSv2, which exhibited lower five-year averaged R^2 values. Last, NARR exhibited the lowest R^2 values among the four datasets at nearshore sites. For offshore sites, ERA5 exhibited the largest R^2 values across the four datasets, with similar values of 0.80 at Sites 3, 4, 5, and 6. This was followed by HRDPS, CFSv2, and NARR exhibiting R^2 values of 0.77, 0.74, 0.60, respectively. Seasonal variations observed in R^2 were more pronounced at nearshore sites compared to offshore sites, where the R^2 values tended to decrease during the spring and summer months and increase during the fall and winter months.

Although the metrics vary by Site and season, several common characteristics do exist by groupings of Sites. At nearshore sites, HRDPS consistently demonstrated the best performance among the four datasets for all metrics. In contrast, results slightly varied across the different metrics at offshore sites. For RMSE, MAE, and R^2, ERA5 outperformed all other datasets in having the most number of months where the metrics exhibited the best values representative of dataset performance. Although CFSv2 emerged as the best overall performer for bias at most sites, ERA5 also exhibited strong performance, ranking as the second-best dataset performer for this metric.

To further assess nearshore versus offshore Site groups, all observed wind speed data over the 5-year period was aggregated per group (i.e., inshore and offshore). Each metric was subsequently calculated using the aggregated data to yield a five-year averaged value per dataset.

Performance was found to be higher for wind speed in the offshore site group, as indicated by lower median absolute values of RMSE, bias, and MAE, and higher R^2, compared to the nearshore site group (Figure 5). The lower performance of the datasets at nearshore sites was likely due to a more complex dynamic environment, where land-sea interactions introduce additional challenges for modeling. However, the wider spread of RMSE, bias, and MAE for offshore sites, with the exception of MAE for ERA5, suggested that dataset performance exhibited greater variability offshore (Figure 5 a–c). In contrast, R^2

https://doi.org/10.5194/wes-2025-57
Preprint. Discussion started: 8 April 2025
© Author(s) 2025. CC BY 4.0 License.

WIND ENERGY SCIENCE DISCUSSIONS

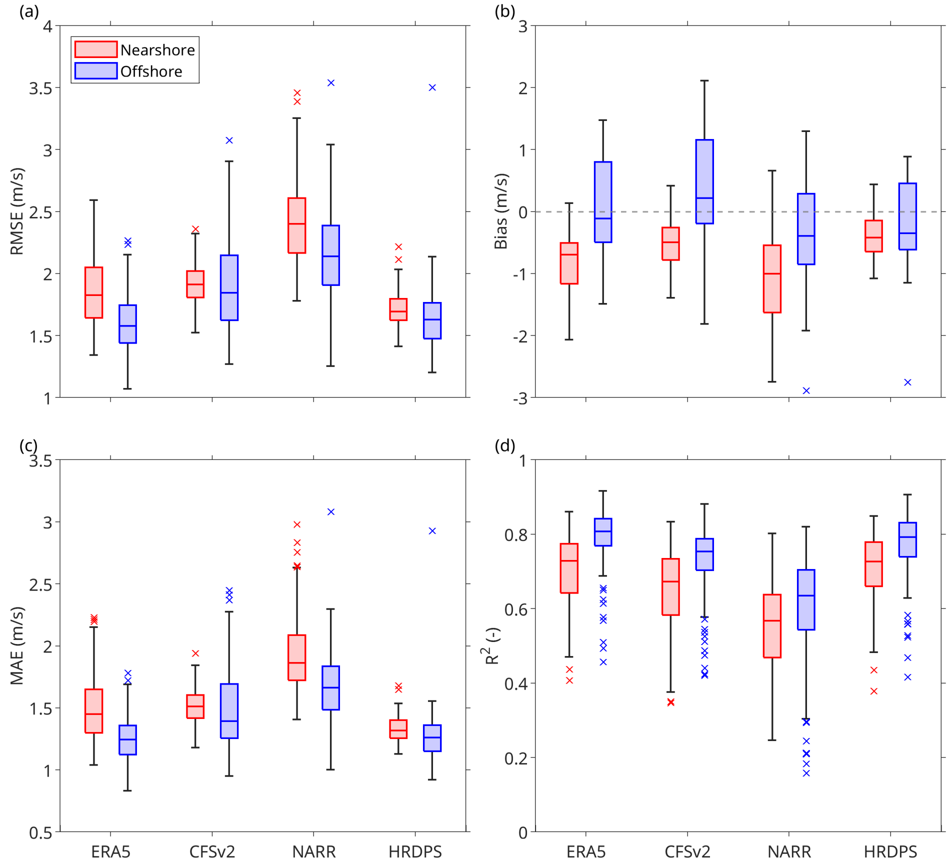

Figure 5. Box charts summarizing the monthly values of four wind speed evaluation metrics, as shown in Figure 4, of (a) RMSE, (b) bias, (c) MAE, and (d) R^2 for the four wind datasets of ERA5, CFSv2, NARR, and HRDPS. Sites are categorized into (red) nearshore and (blue) offshore groups. Each box spans the first and the third quartiles of the data, with the horizontal line inside each box indicating the median value. The whiskers extending from the box represent the minimum and maximum values that are within the 1.5 times the interquartile range (IQR). The individual markers represent the outliers, defined as values exceeding 1.5 times the IQR.

showed a narrower interquartile range (IQR) offshore than nearshore, indicating more consistent correlations between observed and modeled wind speeds in offshore environments (Figure 5 d).

Among the four datasets, HRDPS and ERA5 consistently ranked as the top two performers, each achieving either the best or second-best values across most metrics for both nearshore and offshore site groups. For the nearshore site group, HRDPS emerged as the top-performing dataset, achieving the best mean values for all metrics (Table 3) and the best median values for RMSE, bias, and MAE (Figure 5). While ERA5 held the highest median R^2, HRDPS closely followed with the second-best median value (Figure 5 d). Additionally, HRDPS exhibited the narrowest IQRs for all four metrics, which suggested greater consistency in performance compared to the other datasets (Figure 5). ERA5 ranked second, with the second-best median and

https://doi.org/10.5194/wes-2025-57
Preprint. Discussion started: 8 April 2025
© Author(s) 2025. CC BY 4.0 License.
eawe european academy of wind energy
Open Access WIND ENERGY SCIENCE DISCUSSIONS

mean values for RMSE and MAE (Figure 5 a and c; Table 3), as well as the highest median and second-highest mean value for
320 R^2 (Figure 5 d; Table 3).

Table 3. Mean values of the monthly metrics for wind speed over the 5-year period from January, 2019 to December, 2023. Sites were grouped into nearshore and offshore groups. Only wind speed data within the range of 2–17 m/s were considered. The best-performing dataset metric is highlighted in bold. (-) = no units, as a dimensionless metric.

Metric	ERA5	CFSv2	NARR	HRDPS
		Nearshore		
RMSE (m/s)	1.89	1.92	2.43	**1.72**
Bias (m/s)	-0.81	-0.49	-1.06	**-0.38**
MAE (m/s)	1.49	1.51	1.92	**1.33**
R^2 (-)	0.73	0.69	0.58	**0.75**
		Offshore		
RMSE (m/s)	**1.62**	1.98	2.15	1.64
Bias (m/s)	0.15	0.50	-0.27	**-0.13**
MAE (m/s)	**1.26**	1.52	1.65	1.26
R^2 (-)	**0.80**	0.74	0.66	0.79

For the offshore site group, ERA5 and HRDPS exhibited similarly strong performance, with closely matched median and mean values across all metrics. ERA5 achieved the best median values for all four metrics, while HRDPS ranked second for RMSE, MAE, and R^2 (Figure 5). In terms of mean values, ERA5 achieved the best values for RMSE, MAE, and R^2, and second-best value for bias, while HRDPS achieved the best mean bias and second-best values for the other three metrics
325 (Table 3). Additionally, both ERA5 and HRDPS showed narrower IQRs for RMSE, MAE, and R^2 compared to CFSv2 and NARR, which suggested greater consistency in their offshore performance (Figure 5 a, c and d).

Domestic electricity consumption often fluctuates throughout the day and varies by season. Therefore, wind dataset evaluations should align with these timescales to accurately capture variability and to better inform wind energy development. To achieve this, this study aggregated local hourly wind speed data over the five-year period (January 1, 2019 to December 31,
330 2023) (Figure 6). Data recorded at the same local hour on different days within the same calendar month, across all five years and all six sites, were grouped together for analysis. This approach provided insight into both diurnal and seasonal variations.

Based on RMSE, it was found that wind speed estimation error varied by hour of the day and by month (Figure 6 a). The RMSE exhibited clear seasonal variations for all four datasets, with lower values observed in the spring and summer months (i.e., April to September) and higher values observed in the fall and winter months (i.e., October to March). In contrast, diurnal
335 variation in RMSE appeared to differ between datasets. For ERA5, CFSv2, and NARR, RMSE values tended to peak between 15:00 and 18:00 in all months (except January for CFSv2 and February for NARR), relative to the dataset's mean RMSE for the corresponding month. Additionally, RMSE values for ERA5 and CFSv2 were generally lower between 20:00 and 22:00,

https://doi.org/10.5194/wes-2025-57
Preprint. Discussion started: 8 April 2025
© Author(s) 2025. CC BY 4.0 License.

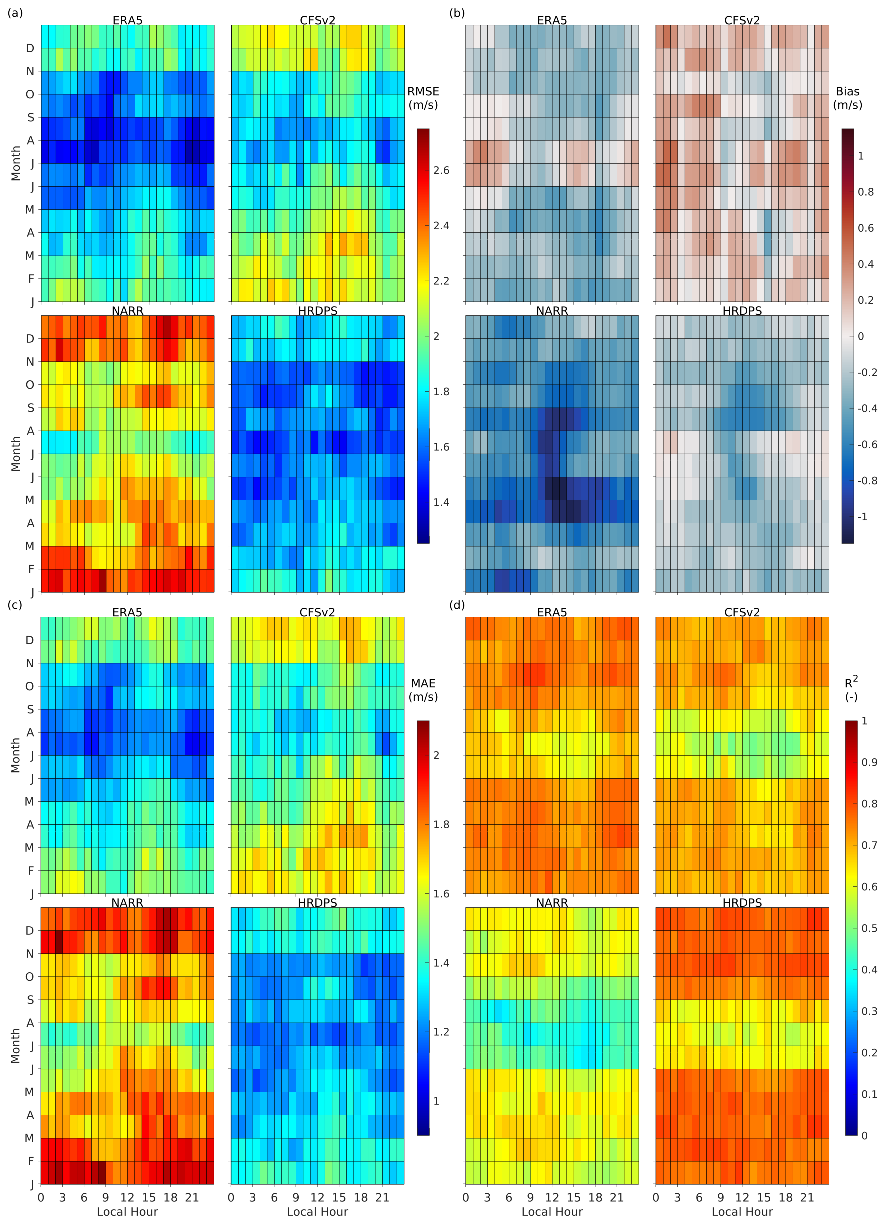

Figure 6. Pseudocolour plots displaying diurnal (local hour) and seasonal (monthly) wind speed variations in (a) RMSE, (b) bias, (c) MAE, and (d) R^2 for each dataset and grouped observation sites from January 1, 2019, to December 31, 2023. The x-axis represents local hours and the y-axis represents months aggregated over the 5 years. Each wind dataset is indicated at the top of each subplot. The wind dataset is indicated at the top of each subplot.

https://doi.org/10.5194/wes-2025-57
Preprint. Discussion started: 8 April 2025
© Author(s) 2025. CC BY 4.0 License.

except in September. In contrast, HRDPS displayed low RMSE values between 12:00 and 15:00 for all months except July. These results highlight the dataset-dependent nature of wind speed estimation errors and emphasize the influence of seasonal and diurnal cycles on dataset performance.

The HRDPS generally had the lowest RMSE values across most months, indicating better wind speed estimation for this metric. ERA5 showed lower RMSE than HRDPS in July and August, but had slightly higher RMSE from November to April. In other months, the RMSE values for ER5 and HRDPS were comparable. CFSv2 performed within a mid-range, while NARR consistently exhibited the highest RMSE values; exhibiting a poorer performance compared to HRDPS and ERA5 for this metric. Overall, winter months displayed the most significant errors in wind speed estimation; particularly, during certain local hours (e.g., between 15:00 and 18:00).

Seasonality in the NARR and HRDPS datasets was evident in the bias metric, which exhibited a higher negative bias during the spring and summer months for NARR and during fall months for HRDPS (Figure 6 b). These negative biases were indicative of significant underestimations of observed wind speeds during these seasons. The bias for ERA5 was generally low, but did exhibit positive values in June and July and negative values during other months. The CFSv2 exhibited an overall positive bias, but lacked a clear seasonal trend. Diurnal variations were notable in some months across all four datasets. For ERA5, the bias during summer months was negative in the morning and positive throughout the remainder of the day. For CFSv2, the bias shifted toward negative values at different times across the months: from 14:00 to 18:00 in March and April, 9:00 to 12:00 in May to July, and 9:00 to 17:00 in August to October. Similarly, NARR and HRDPS exhibited a more pronounced negative bias during midday hours in spring and summer months.

In general, NARR bias was consistently negative across all months and hours of the day, suggesting a systematic underestimation of wind speeds. This underestimation was particularly significant during the spring and summer months and midday (10:00 to 14:00). In contrast, ERA5 exhibited a modest bias overall, with slight overestimations observed in June and July and underestimations observed during the fall and winter months. Diurnal variations were also evident, with higher negative values observed during mid-day and lower negative (or even slightly positive values) observed in the early-morning and late-evening. HRDPS exhibited minimal bias across most months and hours, with relatively larger underestimations observed from August to October; particularly, during mid-day hours. Last, CFSv2 generally exhibited positive bias, but lacked significant seasonal or diurnal variation, suggesting relatively-stable deviations from observations across all time periods.

The MAE exhibited similar seasonal and diurnal patterns as those for RMSE, due to an inherent similarity between these two metrics (Figure 6 c). For R^2, ERA5 and HPDPS generally exhibited higher values compared to the other two datasets (Figure 6 d). Additionally, R^2 values were observed to be lower in the months from June to August.

3.2 Assessment of Wind Direction

While wind speed is the primary factor influencing electricity production in wind farms, wind direction also plays an important role due to its impact on turbine wakes (Gaumond et al., 2014; Stieren et al., 2021). Variation in wind direction for the same turbine layout can lead to differing wake interactions, which can affect downstream turbines and significantly influence total power output. In order to better understand the performance of the four datasets, this study compared the ability of the wind

https://doi.org/10.5194/wes-2025-57
Preprint. Discussion started: 8 April 2025
© Author(s) 2025. CC BY 4.0 License.

model datasets to replicate observed patterns in wind direction. The analysis was similar to that for wind speed described above, with the same performance evaluation metrics being used.

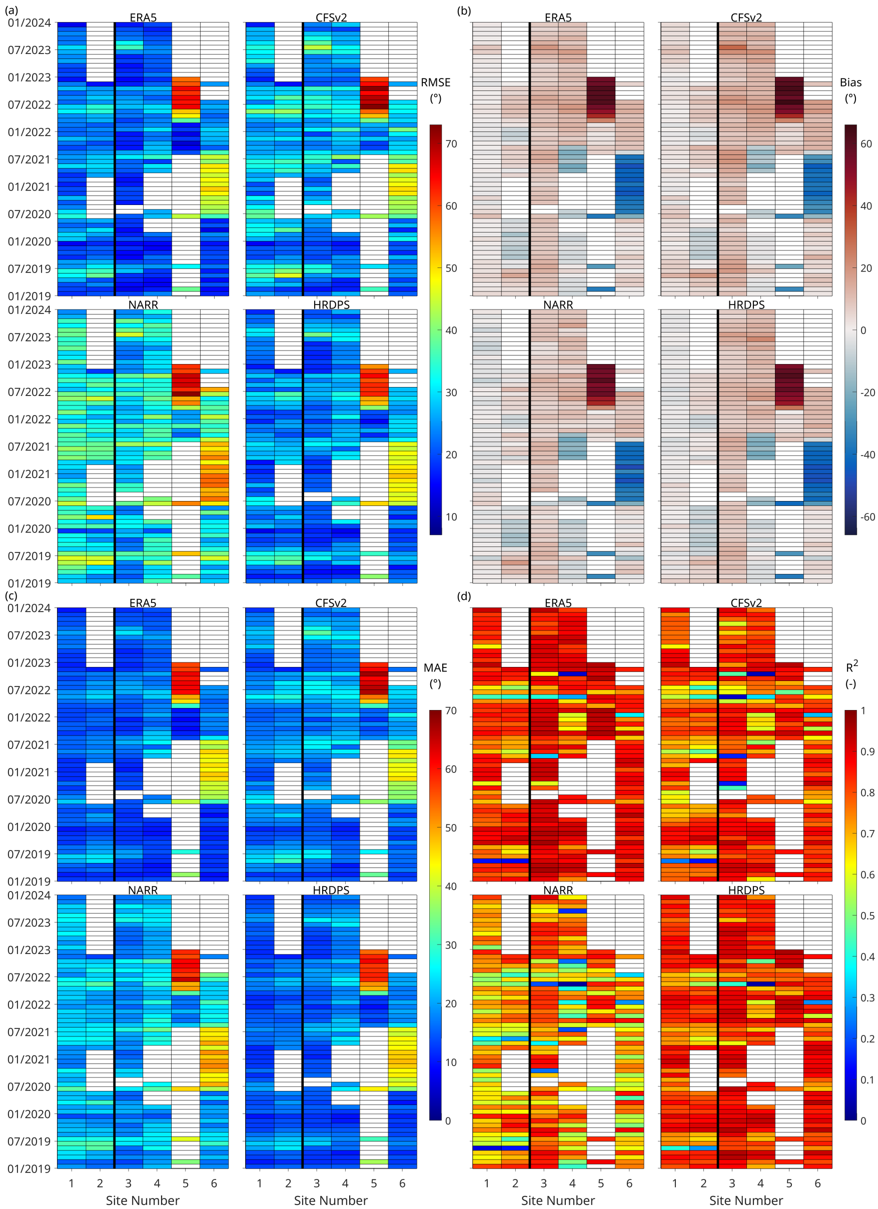

Figure 7. Pseudocolour plots displaying monthly (a) RMSE (b) bias (c) MAE and (d) R^2 for wind direction for each dataset per wind observation site from January 1, 2019, to December 31, 2023. Sites 1 and 2 are representative of the nearshore (left of bold black line in each subplot) and Sites 3-6 are representative of the offshore (right of bold black line in each subplot) on the Scotian Shelf. The wind dataset is indicated at the top of each subplot. Blank areas (white pixels) indicate months and sites that had insufficient, valid observation records (considered to be less than 120 observation records in a month). These were considered to be non-valid for purposes of this study.

https://doi.org/10.5194/wes-2025-57
Preprint. Discussion started: 8 April 2025
© Author(s) 2025. CC BY 4.0 License.

The RMSE for wind direction exhibited clear seasonal patterns, with its value consistently being lower during the winter months (i.e., December to February) compared to summer months (i.e., June to August) across all datasets (Figure 7 a). For nearshore sites, ERA5 exhibited five-year averaged RMSE values of 23.38° ± 4.41° at Site 1 and 25.30° ± 5.04° at Site 2. HRDPS performed similarly to ERA5, which exhibited only slightly higher five-year averaged RMSE values of 0.3° at both sites compared to ERA5. CFSv2 followed ERA5 and HRDPS, which exhibited slightly higher five-year averaged RMSE values of 3° to 4° when compared to the other two datasets. NARR performed the worst on the basis of the five-year averaged RMSE values, which exhibited values that exceeded those of ERA5 and HRDPS by 7° to 11°, respectively. For offshore sites, ERA5 consistently outperformed the other datasets at all four sites, which exhibited five-year averaged RMSE values of 20.35° ± 4.59°, 22.52° ± 4.56°, 40.26° ± 20.36°, and 29.27° ± 11.85° at Sites 3–6, respectively. The HRDPS followed closely, which exhibited five-year averaged RMSE values approximately 2° to 3° higher than those for ERA5. Last, CFSv2 ranked third, which exhibited five-year averaged RMSE values that were 2° to 6° higher than ERA5, with NARR which again exhibited the largest five-year averaged RMSE values for the offshore that were approximately 7° to 11° greater than those for ERA5.

All datasets exhibited similar wind direction performance for the bias metric. Bias values were generally lower at nearshore sites compared to offshore sites for all datasets (Figure 7 b). For the nearshore, the bias values generally ranged between -7° to 8° at Site 1 and -13° to 12° at Site 2. For the offshore, all datasets tended to overestimate wind direction at Site 3 (the meteorological site on Sable Island), which exhibited bias values ranging from 3° to 15°. For the three offshore sites observed using buoys, there were significant biases during periods, for example from April to December in 2022, which was likely due to systematic observational errors. Aside from certain periods, bias in the offshore was similar among all four datasets.

The MAE values at the nearshore sites for HRDPS and ERA5 were very similar and significantly lower than those for the other two datasets (Figure 7 c). For offshore sites, ERA5 performed the best among the four datasets, with HRDPS closely following. The MAE values for CFSv2 were approximately 2°–4° higher than those for ERA5 at all four offshore sites, while the MAE values for NARR were approximately 3°–8° higher compared to ERA5 at these sites.

The monthly R^2 values (Figure 7 d) were similar between the nearshore and offshore sites, which exhibited a typical value of 0.8. At the nearshore sites, HRDPS exhibited the highest five-year averaged R^2 values of 0.81 ± 0.08, 0.77 ± 0.13 at Sites 1 and 2, respectively. ERA5 followed, which exhibited five-year averaged R^2 values of approximately 0.01 lower compared to HRDPS. CFSv2 subsequently performed worse than ERA5, while NARR exhibited the lowest R^2 values among the four datasets at both sites nearshore. At the four offshore sites, ERA5 exhibited the highest five-year averaged R^2 values among the four datasets that ranged from 0.81 ± 0.16 to 0.89 ± 0.08. This was followed by HRDPS, which exhibited five-year averaged R^2 values approximately 0.01–0.03 lower compared to ERA5. CFSv2 subsequently followed, which exhibited five-year averaged R^2 values 0.04-0.09 lower than those for ERA5, while NARR exhibited the lowest five-year averaged R^2 values that were 0.12–0.18 lower than those for ERA5. Seasonal variations observed in R^2 were similar to those observed from wind speed, with the R^2 values tending to decrease during the spring and summer months and increase during the fall and winter months.

Metric results obtained using aggregated data for each site group for wind direction were presented in Figure 8 and Table 4. The median RMSE and MAE values were similar between the nearshore and offshore groups across all four datasets (Figure 8 a,

https://doi.org/10.5194/wes-2025-57
Preprint. Discussion started: 8 April 2025
© Author(s) 2025. CC BY 4.0 License.

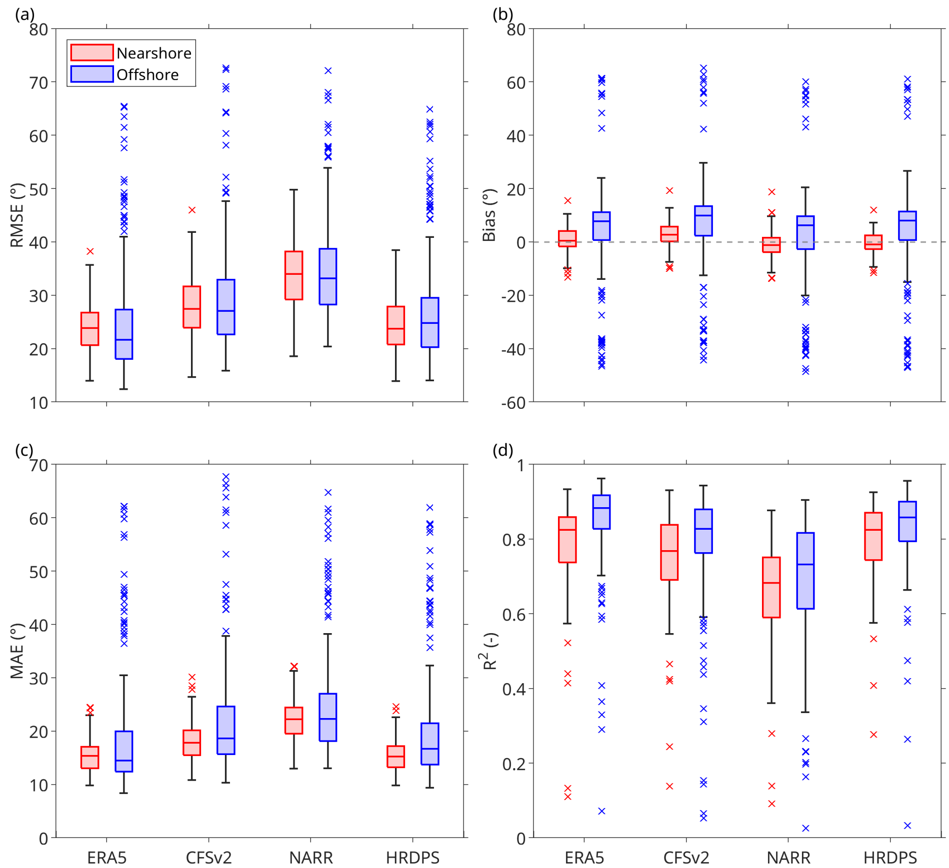

Figure 8. Box charts summarizing the monthly values of four wind direction evaluation metrics, as shown in Figure 7, of (a) RMSE, (b) bias, (c) MAE, and (d) R^2 for the four wind datasets of ERA5, CFSv2, NARR, and HRDPS. Sites are categorized into (red) nearshore and (blue) offshore groups. Each box spans the first and the third quartiles of the data, with the horizontal line inside each box indicating the median value. The whiskers extending from the box represent the minimum and maximum values that are within the 1.5 times the interquartile range (IQR). The individual markers represent the outliers, defined as values exceeding 1.5 times the IQR.

Table 4. Mean values of the monthly metrics for wind direction over the 5-year period from January, 2019, to December, 2023. Sites were grouped into nearshore and offshore groups. Only wind direction data recorded during periods with wind speed in the range of 2–17 m/s were considered. The best-performing dataset metric is highlighted in bold. (-) = no units, as a dimensionless metric.

Metric	ERA5	CFSv2	NARR	HRDPS
		Nearshore		
RMSE (°)	**24.58**	28.59	34.30	24.98
Bias (°)	1.07	2.70	-0.81	**-0.51**
MAE (°)	15.49	18.19	22.33	**15.45**
R^2 (-)	0.81	0.77	0.69	**0.82**
		Offshore		
RMSE (°)	**27.47**	31.40	36.36	29.41
Bias (°)	5.54	8.07	**4.00**	5.18
MAE (°)	**19.09**	22.11	25.02	20.43
R^2 (-)	**0.79**	0.75	0.66	0.77

c), while median bias values were smaller in the nearshore group (Figure 8 b) and median R^2 values were higher offshore (Figure 8 d). The IQRs for bias and MAE were narrower in the nearshore group. In contrast, the IQRs for RMSE and R^2 were comparable between the two groups. Across different datasets, the IQRs were generally similar within each site group.

Similar to the wind speed evaluation, HRDPS and ERA5 ranked as the top two performers for wind direction for both nearshore and offshore site groups. For the nearshore site group, HRDPS and ERA5 exhibited nearly identical best median values across all metrics (Figure 8). In terms of mean values, HRDPS outperformed the other datasets in bias, MAE, and R^2, and achieved the second-best value for RMSE. ERA5 achieved the lowest RMSE and ranked second for MAE and R^2. The only exception was bias, where NARR achieved the second-best mean value instead of ERA5 (Table 4).

For the offshore site group, ERA5 achieved the best median and mean values for RMSE, MAE, and R^2, while HRDPS ranked second for these three metrics in both median and mean values (Figure 8 a, c and d; Table 4). For bias, NARR achieved the best median and mean values, while ERA5 and HRDPS shared the second-best median value, and HRDPS achieved the second-best mean value (Figure 8 b; Table 4).

4 Power Production Simulations for Wind Farm Development Areas

The preceding analysis identified ERA5 and HRDPS as the best performing wind datasets on the Scotian Shelf when compared to regional wind observations. Building upon these findings, this section explored power production simulations within the six PFDAs, using these two datasets.

https://doi.org/10.5194/wes-2025-57
Preprint. Discussion started: 8 April 2025
© Author(s) 2025. CC BY 4.0 License.

4.1 Impact of Turbine Spacing on Wind Farm Performance

Optimizing offshore wind farm layout is a complex process influenced by seabed conditions, environmental impacts, construction feasibility, and wind resource distribution (Hou et al., 2019; Rezaei et al., 2023). The development of offshore wind energy on the Scotian Shelf requires careful consideration of site selection and turbine layout, which currently remain undefined as they depend in part on continued site assessments. To support this process, an idealized scenario was applied in which turbines were uniformly placed within the PFDAs, providing a simplified framework for evaluating potential energy production. Wake effects, caused by turbulence behind turbines, reduces wind speed at downstream turbines and therefore decreases their efficiency. As such, the trade-off between maximizing turbine density and minimizing wake effect wind speed losses is a key consideration in wind farm design.

Table 5. Seasonal mean wind speed (WS) and direction (WD) across six offshore potential future development areas (PFDAs) during winter (December–February) and summer (June–August). The parameters x_{m} and x_{t} represent the values of L/D, obtained from the piecewise function, corresponding to the maximum function value and the transition point between the two segments of the piecewise function, respectively. Refer to Figure 1 for location of PDFAs on the Scotian Shelf.

PFDA	Winter				Summer			
	WS (m/s)	WD (°)	x_m	x_t	WS (m/s)	WD (°)	x_m	x_t
Sydney Bight	10.3	305.0	3.2	3.9	7.4	205.0	3.7	7.8
Canso Bank	9.7	300.0	2.9	4.0	7.3	230.0	3.6	7.5
Eastern Shore	9.3	271.0	3.9	10.0	7.1	231.0	3.6	7.1
Middle Bank	9.7	286.0	3.3	4.3	7.1	235.0	4.3	7.1
Sable Island Bank	9.8	289.0	3.8	4.9	6.8	236.0	5.1	7.7
Emerald Bank	10.0	290.0	3.7	4.7	6.7	237.0	5.0	7.6

To explore how turbine spacing affects the potential total electricity production within the PFDAs, simulations were carried out using PyWake for two seasonal scenarios: winter (December to February) and summer (June to August). To focus on the relationship between total power production and turbine spacing, while reducing computational costs, spatially constant wind speed and wind direction from the ERA5 dataset were used for each seasonal scenario. These values were determined as the spatial and seasonal mean for each PFDA. Winds over the Scotian Shelf are relatively consistent in space, with distinct seasonal patterns. In winter, the seasonal mean wind speed at 10 m height above surface ranged from 9.3 m/s to 10.3 m/s, with wind directions ranging from 271° to 305° across the six PFDAs. In summer, wind speeds ranged from 6.7 m/s to 7.4 m/s, with wind directions ranging between 205° and 237° (Table 5).

The spacing between neighboring turbines was normalized by the rotor diameter as L/D, where L was the distance between two adjacent turbines and D was the rotor diameter. In simulations, L/D was varied incrementally from 2 to 12 in steps of 0.2 to comprehensively assess any impact on energy production. For each spacing configuration, total power output (P_{total}) and power generated per turbine (P_{unit}) were calculated (Figure 9).

https://doi.org/10.5194/wes-2025-57
Preprint. Discussion started: 8 April 2025
© Author(s) 2025. CC BY 4.0 License.

For most of the PFDAs simulated in this study, total electricity production was greatest in winter compared to summer (Figure 9), attributed to the stronger seasonal mean wind speeds observed in winter. However, the Eastern Shore PFDA exhibited a distinct behavior (Figure 9 c), generating higher power in summer regardless of lower wind speeds associated with that season. This was attributed to the PFDA's irregular shape (Figures A2 c and A3 c; note different speed scales in these figures). During summer, the prevailing wind direction in the Eastern Shore PFDA was from southwest (231°), aligning with its narrow span. This configuration reduced wake effects, as fewer turbines were positioned directly downstream of others. In winter, the wind direction shifted to be from the west (271°), flowing more broadly across the PFDA's span. This resulted in increased wake interactions, as more turbines were aligned in the downstream path, thus leading to a greater reduction in power generation. It was noted that this special case of power production being higher in summer than in winter for the Eastern Shore PFDA was specific to simulations with constant wind speed and direction.

The curves of P_{unit} revealed the average turbine efficiencies for the six PFDAs during winter and summer. The results indicated that turbine efficiency improved as L/D increased due to reduced wake effects. In winter, turbines reached their rated capacity of 15 MW when L/D exceeded approximately 4 in most PFDAs, except for the Eastern Shore PFDA given its irregular shape that caused more pronounced wake interactions in winter. In summer, P_{unit} increased more gradually with turbine spacing, following an asymptotic trend. A larger L/D value was required for turbines to achieve a higher wake efficiency. Specifically, to reach a wake efficiency of 0.8, as defined in (6), the minimum values of L/D ranged from 6.4 to 9.0 across the six PFDAs.

Simulated flow maps from the Middle Bank PFDA illustrated wind speed and wake effects during the winter and summer months (Figure 10). In this example, seasonal mean wind speed and wind direction at 10 m height above surface were 9.3 m/s and 271°, respectively, in winter, and 7.1 m/s and 231°, respectively, in summer. Wind speeds were extrapolated to a hub height of 150 m above surface using (1) and turbine spacing set to 3.8 D. Winds within the PFDA were stronger and hence produced higher energy in the winter (Figure 10 b) than in the summer (Figure 10 a).

The flow maps revealed some key features, such as areas of significant wind speed reduction directly behind turbines (represented by the dark shaded regions) and areas where wakes began to dissipate and recover (represented by the lighter tails extending downstream) (Figure 10 a and b). The interaction of wakes from multiple turbines were notable in the interior of the Middle Bank PFDA, where overlapping wake regions created more complex wind speed deficits. This clustering of wake effects appeared to cause downstream turbines to experience more pronounced reductions in wind speed due to the cumulative impact of upstream wakes. When turbine spacing was set to 9.6 D, and wind parameters for winter were assumed, impact of wakes caused by upstream turbines on downstream turbines appeared negligible (Figure 10 c and d).

Wake-turbine interactions caused reduced power production for turbines differently depending on turbine locations and wind directions. Figure 11 (a) presented the spatial distribution of seasonally-averaged power production of individual wind turbines for the six PFDAs.

Simulations were conducted using hourly wind data from the ERA5 dataset. The hourly power output of each turbine was averaged over the respective 5-year winter and summer periods from 2019 to 2023. Two turbine spacing scenarios were considered. The first was a dense layout with normalized spacings, L/D, ranged from 3.3 to 4.5 across the six PFDAs (Table 6). The corresponding spacing in each PFDA represented the average where power production peaked in two seasons under a

https://doi.org/10.5194/wes-2025-57
Preprint. Discussion started: 8 April 2025
© Author(s) 2025. CC BY 4.0 License.

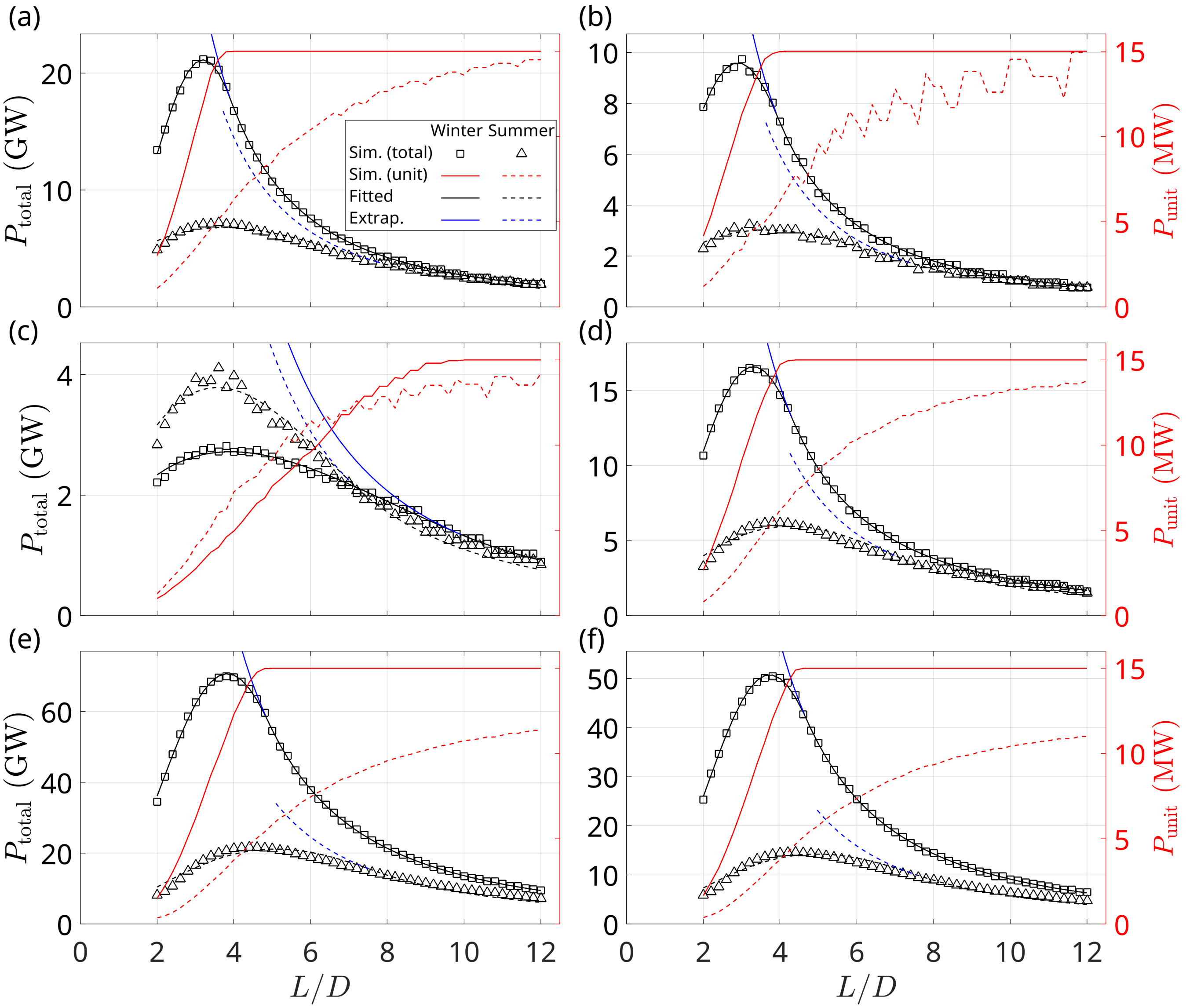

Figure 9. Relationships between total power production, P_{total} (Y-axis on the left), and normalized turbine spacings (L/D) for the six potential future development areas (PFDAs) of (a) Sydney Bight, (b) Canso Bank, (c) Eastern Shore, (d) Middle Bank, (e) Sable Island Bank, and (f) Emerald Bank. Rectangular markers (□) and triangular markers (△) represent simulation results for winter and summer, respectively. The black solid and dashed curves are fitted piecewise functions for winter and summer, respectively. The Y-axis on the right shows power production per turbine, P_{unit}, from simulations for winter (solid red lines) and summer (dashed red lines). Last, the blue curves show extrapolation of the inverse square part of the piecewise function for $L/D < x_{\text{t}}$, which is described further in Section 4.2 below. Refer to Figure 1 for location of PFDAs on the Scotian Shelf.

https://doi.org/10.5194/wes-2025-57
Preprint. Discussion started: 8 April 2025
© Author(s) 2025. CC BY 4.0 License.

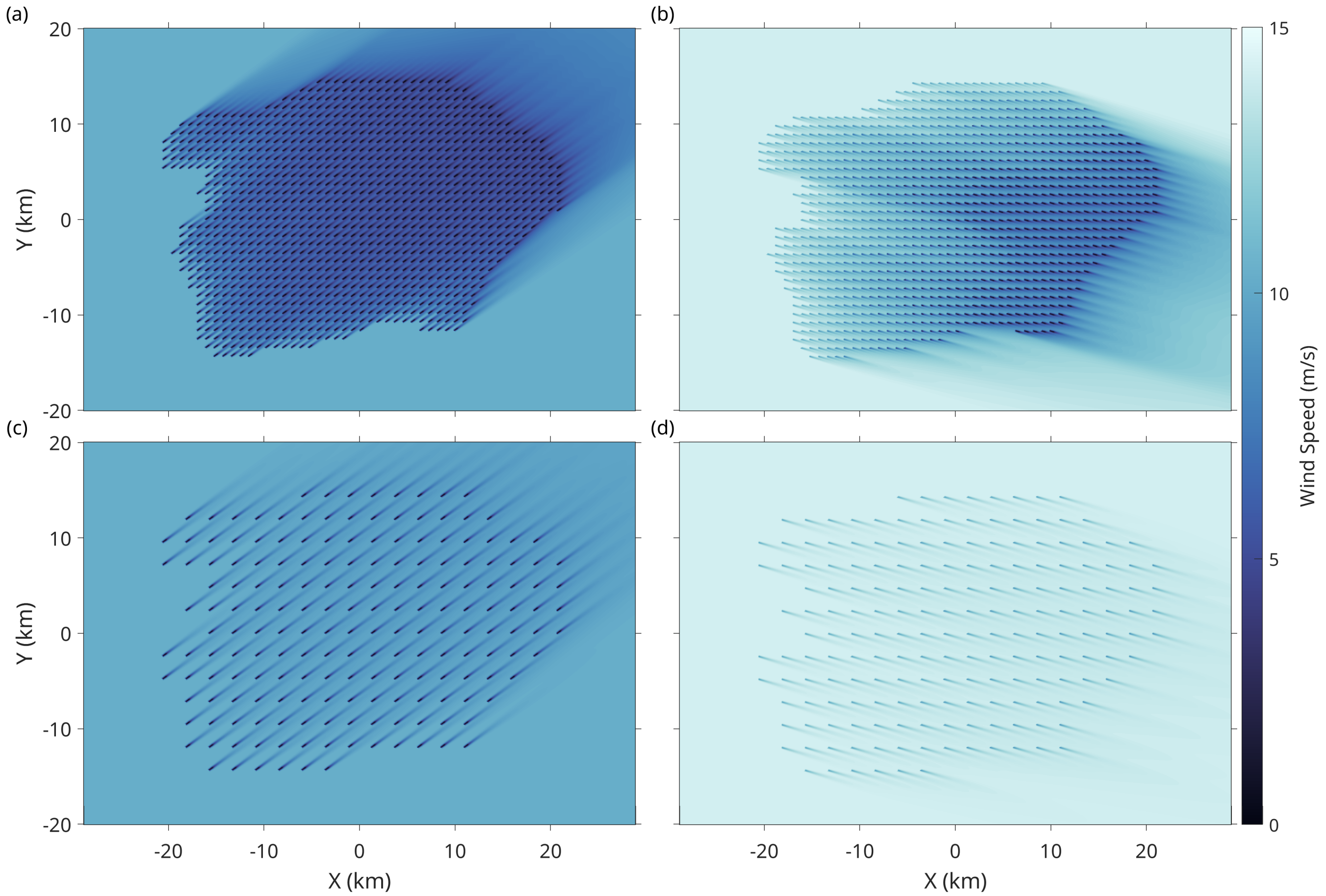

Figure 10. Flow maps of wind speed and wake effects simulated using PyWake for the Middle Bank potential future development area (PFDA) during (a, c) summer and (b, d) winter. The assumed turbine spacings were (a, b) 3.8 and (c, d) 9.6 times the rotor diameter, approximately 0.9 km and 2.3 km, respectively. Wind data used in the simulation corresponded to the seasonal mean wind speed and wind direction at 10 m height above surface using the ERA5 dataset. These were 9.3 m/s and 271°, respectively, for winter and 7.1 m/s and 231°, respectively, for summer. The input wind data was extrapolated to an assumed turbine hub height of 150 m above surface, with results presented in the figure being at hub height. Refer to Figure 1 for location of the Middle Bank PFDA on the Scotian Shelf.

simplified model with constant wind speed and direction. The second scenario used a uniform spacing of $L/D = 9.6$ for all PFDAs. This spacing represented a scenario where the wake effects were minimal and allowed for approximately 1000 turbines in Sable Island Bank PFDA (Table 7), aligning with estimates from Nicholson (2023). Diagrams illustrating turbine layouts for six PFDAs on the Scotian Shelf were provided in Figure A1.

Wind conditions in the two seasons on the Scotian Shelf were illustrated with the wind rose diagrams using the examples of the Sydney Bight and Middle Bank PFDAs (Figure 11 b). In winter, wind speeds were generally higher, predominantly blowing from the northwest, with frequent occurrences of speeds exceeding 12 m/s. In summer, the winds were weaker, primarily blowing from the southwest, with most speeds falling below 12 m/s.

The turbine spacing and seasonal wind variations significantly influenced the power production of individual turbines at different locations. Under the large spacing scenario ($L/D = 9.6$), wake effects were minimal in both seasons, as evidenced by the relatively uniform power production among turbines within each PFDA (bottom panels in Figure 11 a). In contrast, in the smaller spacing scenario, wake effects became more pronounced and reduced the efficiency of individual turbines (top panels in Figure 11 a).

Power production of individual turbines varied within each PFDA, depending on turbine placement and dominant wind direction. Reviewing the Middle Bank PFDA as an example, in winter, when the prevailing winds were from the northwest, turbines located near the northern and western edges exhibited the highest power production (top-left panel in Figure 11 a). These turbines experienced less wake interference as they were positioned upstream relative to the dominant wind direction. In contrast, during summer, when winds predominantly came from the southwest, the highest power production was observed for turbines situated along the western and southern edges of the PFDA (top-right panel in Figure 11 a). For turbines located further downstream in the interior or at the leeward edges of the PFDA, power production was significantly reduced due to wake effects.

4.2 Simulation Results and Fitting

The simulated total power production, P_{total}, for the six PFDAs during two seasons exhibited a characteristic pattern consisting of two distinct regimes (Figure 9).

In the first regime, where turbine spacing was large and wake losses were negligible, the per-turbine power production approached its theoretical limit depending on the background wind speed (see: Figure 2). Under these conditions, P_{total} for a given PFDA, using the same turbine model, scaled proportionally with the total number of installed turbines. Since the area of each PFDA was fixed, the total number of turbines followed an inverse square relationship with turbine spacing. Consequently, P_{total} exhibited an inverse square relationship with L/D.

In the second regime, where turbine spacing was smaller and wake effects became significant, the simulation results exhibited a non-monotonic trend in P_{total}. Initially, as L/D decreased, P_{total} increased due to the increased number of turbines. However, beyond a critical threshold, further reduction in L/D led to a sharp decline in P_{total} due to intensified wake effects. This bell-shaped pattern was similar to the Weibull-like function.

https://doi.org/10.5194/wes-2025-57
Preprint. Discussion started: 8 April 2025
© Author(s) 2025. CC BY 4.0 License.

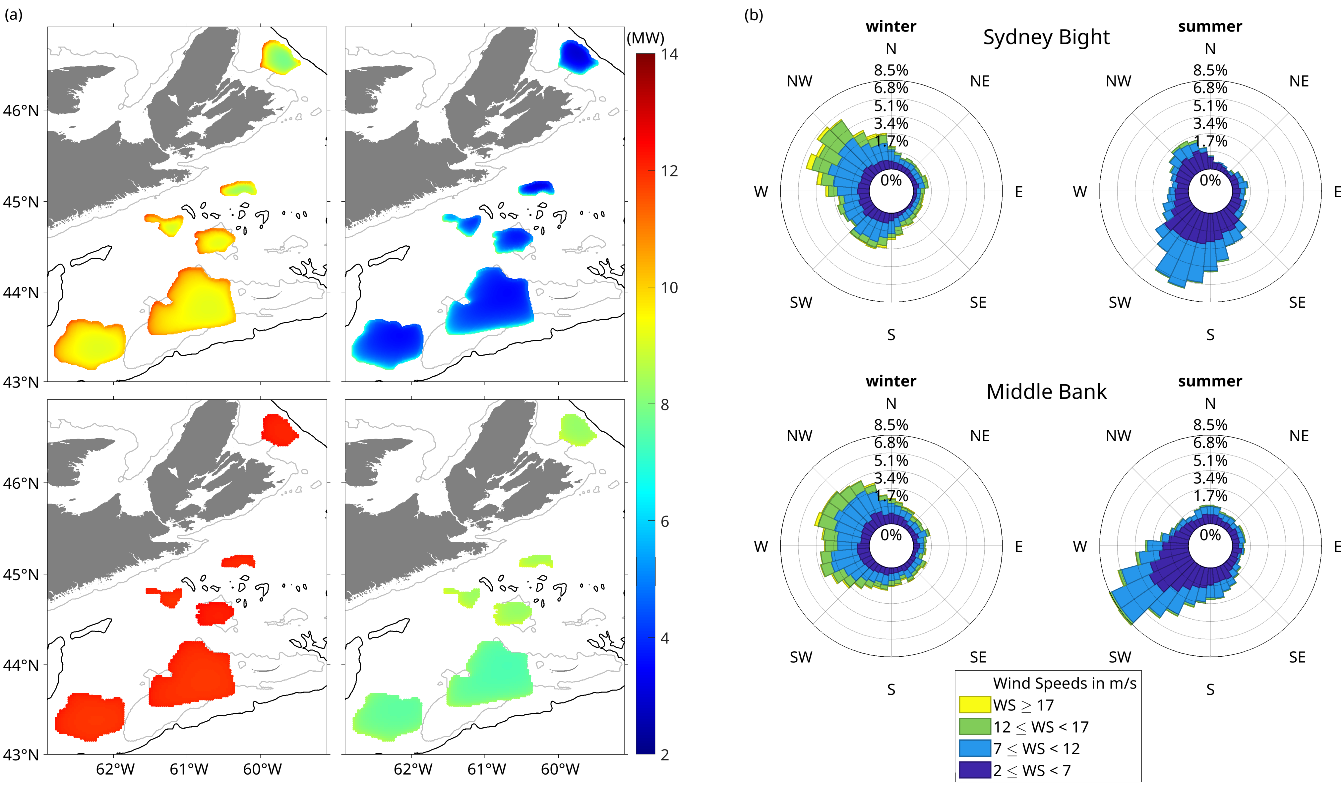

Figure 11. (a) Spatial distribution of wind turbine power production for two turbine layouts and two seasons for all potential future development areas (PFDAs) on the Scotian Shelf. Color shading shows the mean power production for each PFDA, averaged across (left panels) winter and (right panel) summers from 2019 to 2023. Normalized turbine spacing, L/D, ranged from (top panels) 3.3 to 4.5 across the six PFDAs as listed in Table 6, and (bottom panels) $L/D = 9.6$. (b) Wind rose diagrams for (top panels) the Sydney Bight PFDA and (bottom panels) Middle Bank PFDA, based on spatially-averaged ERA5 data from 2019 to 2023. Refer to Figure 1 for location of PFDAs on the Scotian Shelf.

Building on the two-regime behaviours, the simulation results were modeled using an empirical piecewise function for P_{total}
515 as a function of L/D. This function captured the inverse square relationship at large L/D and the Weibull-like behavior at small L/D. This piecewise function was formulated as follows:

$$f(x) = \begin{cases} a \cdot \frac{k}{\lambda}\left(\frac{x}{\lambda}\right)^{k-1} e^{-\left(\frac{x}{\lambda}\right)^k}, & \text{for } x < x_{\mathrm{t}}, \\ \frac{c}{x^2}, & \text{for } x \geq x_{\mathrm{t}}. \end{cases} \tag{7}$$

Here, a, k, and λ were parameters of the Weibull-like function; x_{t} was the critical transition point where the behavior transitions from the Weibull-like regime to the inverse square regime; and c was the coefficient ensuring continuity at $x = x_{\mathrm{t}}$.

520 To ensure a smooth transition between these two regimes at $x = x_{\mathrm{t}}$, the following continuity conditions were applied:

https://doi.org/10.5194/wes-2025-57
Preprint. Discussion started: 8 April 2025
© Author(s) 2025. CC BY 4.0 License.

WIND ENERGY SCIENCE DISCUSSIONS

- Value Continuity:

$$a \cdot e^{-\left(\frac{x_\mathrm{t}}{k}\right)^b} = \frac{c}{x_\mathrm{t}^2}. \tag{8}$$

- Derivative Continuity:

$$-a \cdot \frac{b}{k}\left(\frac{x_\mathrm{t}}{k}\right)^{b-1} e^{-\left(\frac{x_\mathrm{t}}{k}\right)^b} = -\frac{2c}{x_\mathrm{t}^3}. \tag{9}$$

From these conditions, the transition point x_t and the coefficient c were determined analytically as:

$$x_\mathrm{t} = \lambda\left(\frac{k+1}{k}\right)^{1/k}, \tag{10}$$

and

$$c = a \cdot \frac{k}{\lambda}\left(\frac{x_\mathrm{t}}{\lambda}\right)^{k-1} e^{-\left(\frac{x_\mathrm{t}}{\lambda}\right)^k} \cdot x_\mathrm{t}^2. \tag{11}$$

The maximum value of the function was located at:

$$x_\mathrm{m} = \lambda\left(\frac{k-1}{k}\right)^{1/k}. \tag{12}$$

Substituting this value of x_m into the first part of the piecewise function yields the maximum value:

$$f_\mathrm{m} = a \cdot \frac{k}{\lambda}\left(\frac{k-1}{k}\right)^{(k-1)/k} e^{-\left(\frac{k-1}{k}\right)}. \tag{13}$$

This value represents the maximum total power production predicted by the Weibull-like part of the piecewise function.

Parameters of a, λ, and k were unknown, but were obtained through non-linear fitting. In this fitting process, the independent variable, x, represents the normalized turbine spacing, L/D.

The simulation results for six PFDAs in two seasons (Figure 9) were fitted using the piecewise function. The fitted functions were overlaid on the simulation data for comparison. From the fitted functions, the parameters a, λ, and k were determined, allowing for the calculation of x_t and x_m, which were presented in Table 5. The parameter x_m represents the normalized turbine spacing (L/D), at which total power production reaches its maximum for a given PFDA. This value ranged from 2.9 to 3.9 in winter and 3.6 to 5.1 in summer for the six PFDAs.

The parameter x_t defines the transition point at which wake effects become negligible for $L/D > x_\mathrm{t}$, with wake effects becoming significant for $L/D < x_\mathrm{t}$. In winter, x_t ranged from 3.9 to 4.9 for most PFDAs, except for the Eastern Shore PFDA where a different wake interaction pattern was observed. In summer, x_t was notably larger, ranging from 7.1 to 7.8.

The fitted piecewise function was closely aligned with the simulation results. The extrapolated curve for $L/D < x_\mathrm{t}$, based on the inverse square relationship, was shown in blue (Figure 9). The difference between the extrapolated curves and the fitted piecewise function illustrated power production losses due to wake effects. These losses were more pronounced in summer than in winter for most PFDAs, except for the Eastern Shore PFDA.

https://doi.org/10.5194/wes-2025-57
Preprint. Discussion started: 8 April 2025
© Author(s) 2025. CC BY 4.0 License.

4.3 Temporal Variations in Simulated Electricity Production

Ttotal electricity production for the PFDAs on the Scotian Shelf were more accurately estimated by using time-dependent wind speeds and wind directions. After reviewing earlier assessments of wind datasets, the ERA5 and HRDPS datasets were selected for use in this study. Because spatial variation in wind within each PFDA domain was minimal, wind speeds and wind directions were averaged across each area. Before running simulations, wind speed at 10 m above surface was converted to a wind speed at turbine hub height of 150 m above surface. Two scenarios for turbine spacings (L/D) were then tested: 1) values ranging from 3.3 to 4.5 L/D across the six PFDAs (see Table 6), which were obtained as the mean values of x_m in winter and summer (Table 5); and 2) a fixed turbine spacing of L/D = 9.6.

Uncertainty in power estimation associated with the RMSE between wind datasets and wind observations was also accounted for. For each dataset, two synthetic wind speed time series were generated by adding or subtracting the RMSE from the 10 m wind speeds, then separate simulations were run using the data. The resulting power values represented the upper and lower bounds of the uncertainty range. For total power without wake effects, a single-turbine power curve was used (Figure 2), which was then multiplied by the number of turbines. Hourly time series of total power for the six PFDAs were obtained from the simulations, which were then time-averaged to create a monthly time series (Figure 12). Seasonal mean results in winter and summer were summarized in Table 6. Since the results obtained with ERA5 and HRDPS were very similar, the following description only refers to that obtained using the ERA5 dataset.

For the six PFDAs, total electricity production rates ranged from 6.1 to 3.4 GW, for the winter and summer, respectively, at the smallest PFDA (Eastern Shore) to 44.6 to 20.2 GW, for the winter and summer respectively, at the largest PFDA (Sable Island Bank) (Table 6). All six PFDAs exhibited clear seasonal cycles, with higher energy production observed during winter months (December to February) and lower energy production observed during summer months (June to August). For example, at the Middle Bank PFDA, the total power production observed in winter (11.2 $\pm$ 2.7 GW, Table 6) was approximately double that observed in summer (5.5 $\pm$ 2.8 GW, Table 6).

In considering results of simulations with a ‘No Wake’ scenario, where total energy production depended only on wind speed and turbine number, the extent of energy loss due to wake effects was revealing. For all six PFDAs, simulation results that accounted for wake effects consistently exhibited energy productions that fell below those of the ‘No Wake’ scenario (Figure 12). Further, wake-induced reductions in electricity production were higher in percentage terms during summer compared to winter. For example, at the Middle Bank PFDA total energy losses associated with wakes were approximately 17% in winter (December to February) compared to 48% in summer (June to August) (Table 6).

Simulations that used the ERA5 and HRDPS datasets generally produced similar total power estimates for larger PFDAs, such as Sydney Bight, Sable Island Bank, and Emerald Bank. In contrast, for smaller PFDAs, such as Canso Bank, Eastern Shore, and Middle Bank, the simulated power using ERA5 was slightly higher compared to using HRDPS; particularly, during periods of low energy production (e.g., May to August 2021). As a result, the combined uncertainty bands were wider in summer months due to discrepancies between the two datasets observed during low-production periods.

https://doi.org/10.5194/wes-2025-57
Preprint. Discussion started: 8 April 2025
© Author(s) 2025. CC BY 4.0 License.

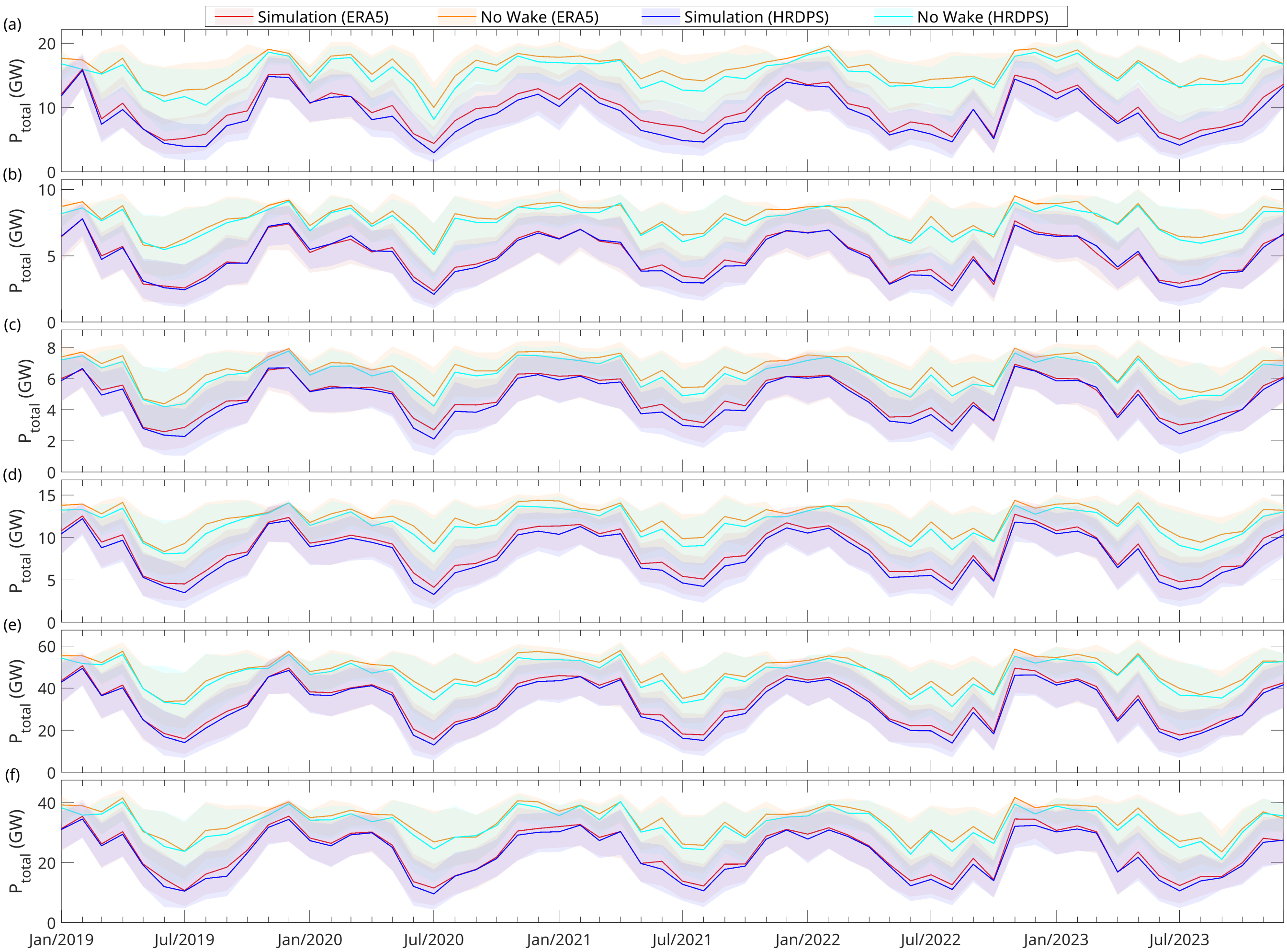

Figure 12. Time series of total power estimated from simulations for the six potential future development areas (PFDAs) of (a) Sydney Bight, (b) Canso Bank, (c) Eastern Shore, (d) Middle Bank, (e) Sable Island Bank, and (f) Emerald Bank using ERA5 and HRDPS wind datasets. The 'No Wake' curves indicate the theoretical maximum energy production without accounting for wake losses. Turbine spacings (L/D) are listed in Table 5. The shaded areas represent uncertainties due to differences in wind speeds between datasets and offshore wind observation sites. The uncertainties are quantified using the RMSE between the dataset and observed wind speeds. Refer to Figure 1 for location of PFDAs on the Scotian Shelf.

https://doi.org/10.5194/wes-2025-57
Preprint. Discussion started: 8 April 2025
© Author(s) 2025. CC BY 4.0 License.

In a scenario where turbine spacing was set to $L/D = 9.6$, seasonal cycles (Figure 13) were consistent with those observed in the scenario with small turbine spacings (Figure 12), which further reinforced that in winter months (December to February) the PFDAs exhibit much higher electricity generation rates compared to summer months (July and August). For example, at the Middle Bank PFDA the total power production observed in winter (2.3 ± 0.4 GW, Table 7) was approximately 44% higher
585 compared to summer (1.6 ± 0.5 GW, Table 7).

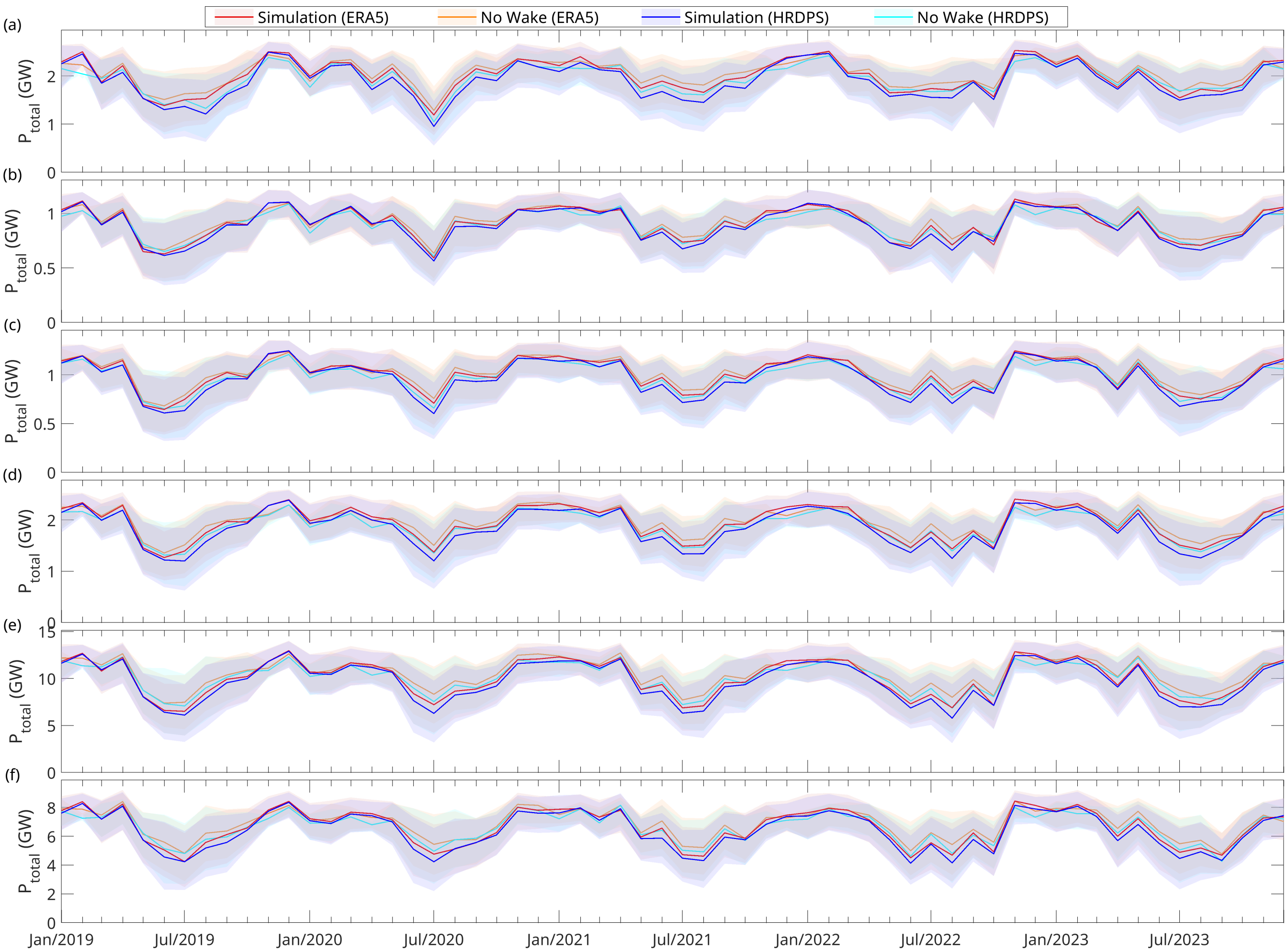

Figure 13. Same simulations described in Figure 12 and Table 6, but with a turbine spacing set to 9.6 times the rotor diameter.

The impact of wake effects across all six areas under the $L/D = 9.6$ turbine spacing scenario (Figure 13, Table 7) was significantly diminished when compared to the scenario with smaller turbine spacing (Figure 12, Table 6). In winter, the simulation results were almost identical to the 'No Wake' case. Interestingly, however, the 'No Wake' case showed slightly lower power outputs than the 'Wake' case simulations for some PFDAs. This occurred in high-wind conditions (winds greater
590 than 25 m/s), where turbines stop operating in the 'No Wake' case, which resulted in zero power output (see: Figure 2). Further,

https://doi.org/10.5194/wes-2025-57
Preprint. Discussion started: 8 April 2025
© Author(s) 2025. CC BY 4.0 License.

Table 6. Seasonal mean values of total power production for the six potential future development areas (PFDAs) in winter (December to February) and summer (June to August) derived from the simulations results shown in Figure 12. Turbine spacings (L/D) and numbers varied across the six PFDAs, and the total number of turbines was determined for each wind farm based on this spacing. Uncertainties are represented by the maximum deviations of the seasonal mean of upper and lower bounds from the mean values.

PFDA	L/D	Turbine Number	P_{total} (GW), ERA5				P_{total} (GW), HRDPS			
			Winter		Summer		Winter		Summer	
			Wake	No Wake	Wake	No Wake	Wake	No Wake	Wake	No Wake
Sydney Bight	3.5	1515	13.3 ± 3.7	17.9 ± 2.3	6.2 ± 3.4	13.8 ± 4.4	12.8 ± 3.4	17.2 ± 2.4	5.0 ± 3.5	12.6 ± 4.7
Canso Bank	3.3	731	6.7 ± 1.8	8.7 ± 1.3	3.3 ± 1.7	6.7 ± 2.1	6.7 ± 1.6	8.4 ± 1.0	3.0 ± 1.8	6.4 ± 2.3
Eastern Shore	3.7	623	6.1 ± 1.5	7.4 ± 1.1	3.4 ± 1.6	5.7 ± 1.8	6.0 ± 1.4	7.2 ± 1.0	3.0 ± 1.7	5.2 ± 2.0
Middle Bank	3.8	1136	11.2 ± 2.7	13.5 ± 1.6	5.5 ± 2.8	10.4 ± 3.3	10.7 ± 2.4	13.1 ± 1.7	4.7 ± 2.9	9.5 ± 3.6
Sable Island Bank	4.5	4569	44.6 ± 10.6	54.2 ± 6.8	20.2 ± 11.0	39.7 ± 13.5	43.4 ± 9.7	52.2 ± 6.5	17.9 ± 11.4	37.3 ± 14.5
Emerald Bank	4.3	3226	31.3 ± 7.3	38.0 ± 4.7	14.3 ± 8.0	28.3 ± 9.7	30.5 ± 6.8	36.9 ± 4.7	12.8 ± 8.4	26.7 ± 10.3

Table 7. Seasonal mean values of total power production for the six potential future development areas (PFDAs) in winter (December to February) and summer (June to August) derived from the simulation results shown in Figure 13. Turbine spacing (L/D) was fixed for the six PFDAs and the total number of turbines was determined for each wind farm based on this spacing. Uncertainties are represented by the maximum deviations of the seasonal mean of the upper and lower bounds from the mean values.

PFDA	L/D	Turbine Number	P_{total} (GW), ERA5				P_{total} (GW), HRDPS			
			Winter		Summer		Winter		Summer	
			Wake	No Wake	Wake	No Wake	Wake	No Wake	Wake	No Wake
Sydney Bight	9.6	194	2.4 ± 0.4	2.3 ± 0.3	1.6 ± 0.6	1.8 ± 0.6	2.3 ± 0.4	2.2 ± 0.3	1.5 ± 0.6	1.6 ± 0.6
Canso Bank	9.6	87	1.0 ± 0.2	1.0 ± 0.2	0.8 ± 0.2	0.8 ± 0.3	1.0 ± 0.2	1.0 ± 0.1	0.7 ± 0.3	0.8 ± 0.3
Eastern Shore	9.6	97	1.2 ± 0.2	1.2 ± 0.2	0.8 ± 0.3	0.9 ± 0.3	1.1 ± 0.2	1.1 ± 0.2	0.8 ± 0.3	0.8 ± 0.3
Middle Bank	9.6	185	2.3 ± 0.4	2.2 ± 0.3	1.6 ± 0.5	1.7 ± 0.5	2.2 ± 0.4	2.1 ± 0.3	1.4 ± 0.6	1.5 ± 0.6

https://doi.org/10.5194/wes-2025-57
Preprint. Discussion started: 8 April 2025
© Author(s) 2025. CC BY 4.0 License.

in the simulations the wake effects were observed to reduce wind speeds in the interior of PFDAs to less than 25 m/s, which allowed the turbines in the interior areas to continue producing power. In summer, the 'Wake' case simulations generally produced slightly lower power than the 'No Wake' case. For instance, at the Middle Bank, simulated power output (1.6 ± 0.6 GW with ERA5 in Table 7) was only about 6% less than that of the 'No Wake' case (1.7 ± 0.5 GW with ERA5 in Table 7).

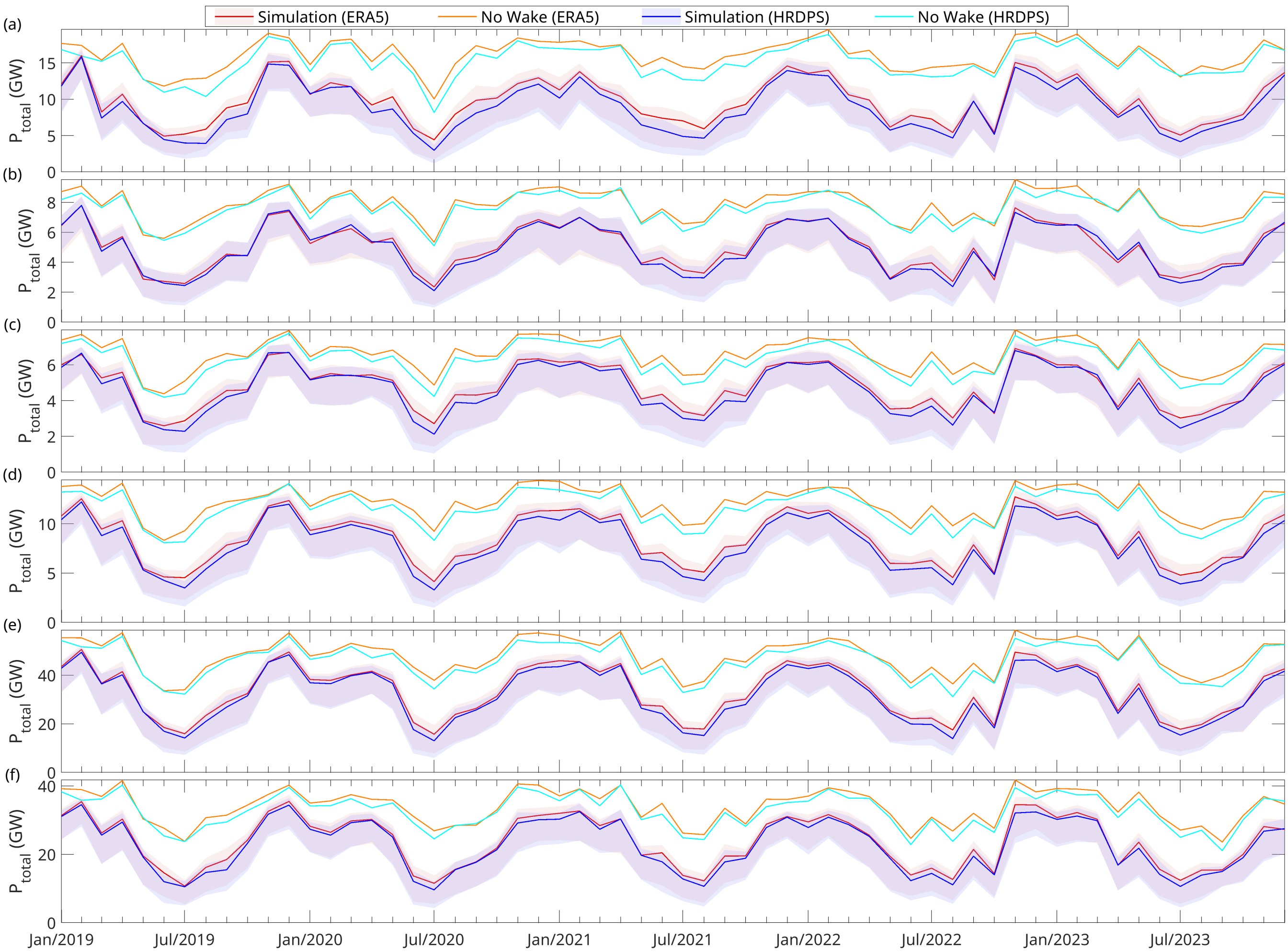

Figure 14. Same simulations described in Figure 12 and Table 6, except that the uncertainties are estimated to account for the wind direction estimation errors.

595 Uncertainties in power estimation arising from wind direction errors between datasets and observations were also accounted for in this analysis. To quantify these uncertainties, separate simulations were conducted using wind directions perturbed based on dataset-specific error characteristics. Unlike wind speed, which has a monotonic relationship with power production, where an increase or decrease in wind speed directly leads to a corresponding change in power output, wind direction does not

https://doi.org/10.5194/wes-2025-57
Preprint. Discussion started: 8 April 2025
© Author(s) 2025. CC BY 4.0 License.
eawe european academy of wind energy
Open Access WIND ENERGY SCIENCE DISCUSSIONS

Table 8. Seasonal mean values of total power production for the six potential future development areas (PFDAs) in winter (December to February) and summer (June to August) derived from the simulation results shown in Figure 14. Turbine spacings (L/D) varied across the six PFDAs. Uncertainties are represented by the maximum deviations of the seasonal mean of upper and lower bounds from the mean values.

PFDA	L/D	P_{total} (GW), ERA5		P_{total} (GW), HRDPS	
		Winter, Wake	Summer, Wake	Winter, Wake	Summer, Wake
Sydney Bight	3.5	13.3 ± 3.9	6.2 ± 3.2	12.8 ± 3.8	5.0 ± 2.6
Canso Bank	3.3	6.7 ± 1.9	3.3 ± 1.6	6.7 ± 1.8	3.0 ± 1.6
Eastern Shore	3.7	6.1 ± 1.5	3.4 ± 1.6	6.0 ± 1.4	3.0 ± 1.5
Middle Bank	3.8	11.2 ± 2.8	5.5 ± 2.6	10.7 ± 2.6	4.7 ± 2.4
Sable Island Bank	4.5	44.6 ± 10.4	20.2 ± 9.4	43.4 ± 10.0	17.9 ± 8.8
Emerald Bank	4.3	31.3 ± 7.3	14.3 ± 6.9	30.5 ± 7.2	12.8 ± 6.5

influence power generation in a strictly linear manner. Variations in wind direction can alter wake interactions and turbine efficiency in complex ways, making the uncertainty estimation less straightforward.

To estimate the uncertainty of simulated power production caused by the wind direction errors in wind datasets, monthly RMSE values were used as error bounds. For each month, a range of possible wind directions was defined by adding and subtracting the monthly RMSE from the original wind direction time series. Within this range, 10 additional time series of wind directions were generated, where wind directions were evenly distributed between the upper and lower bounds. Simulations were then conducted using these 10 perturbed time series along with the original time series, resulting in a total of 11 simulations per dataset. At each hour, the uncertainty in power production was defined by the minimum and maximum values obtained from the 11 simulations.

In the dense layout scenario, uncertainties of power production resulting from wind direction estimation errors (Figure 14 and Table 8) were comparable in magnitude to those caused by wind speed estimation errors (Figure 12 and Table 6). However, in the $L/D = 9.6$ scenario, the impact of wind direction errors (Figure 15 and Table 9) was less significant compared to the uncertainties introduced by wind speed errors (Figure 13 and Table 7).

5 Discussion

Offshore wind energy holds significant promise in the global transition from fossil fuels to clean energy. The Scotian Shelf is recognized for its world-class wind resources (Nicholson, 2023; Government of Nova Scotia, 2023), presenting a significant opportunity for offshore wind farm development that has now been embedded in the federal and provincial energy strategies (Government of Nova Scotia, 2023; Canada, n.d.). Motivated by a need to better understand wind energy potential in the Scotian Shelf offshore area, this study focused on two primary aspects: assessment of wind datasets and estimation of potential power production in six PFDAs on the Scotian Shelf.

https://doi.org/10.5194/wes-2025-57
Preprint. Discussion started: 8 April 2025
© Author(s) 2025. CC BY 4.0 License.

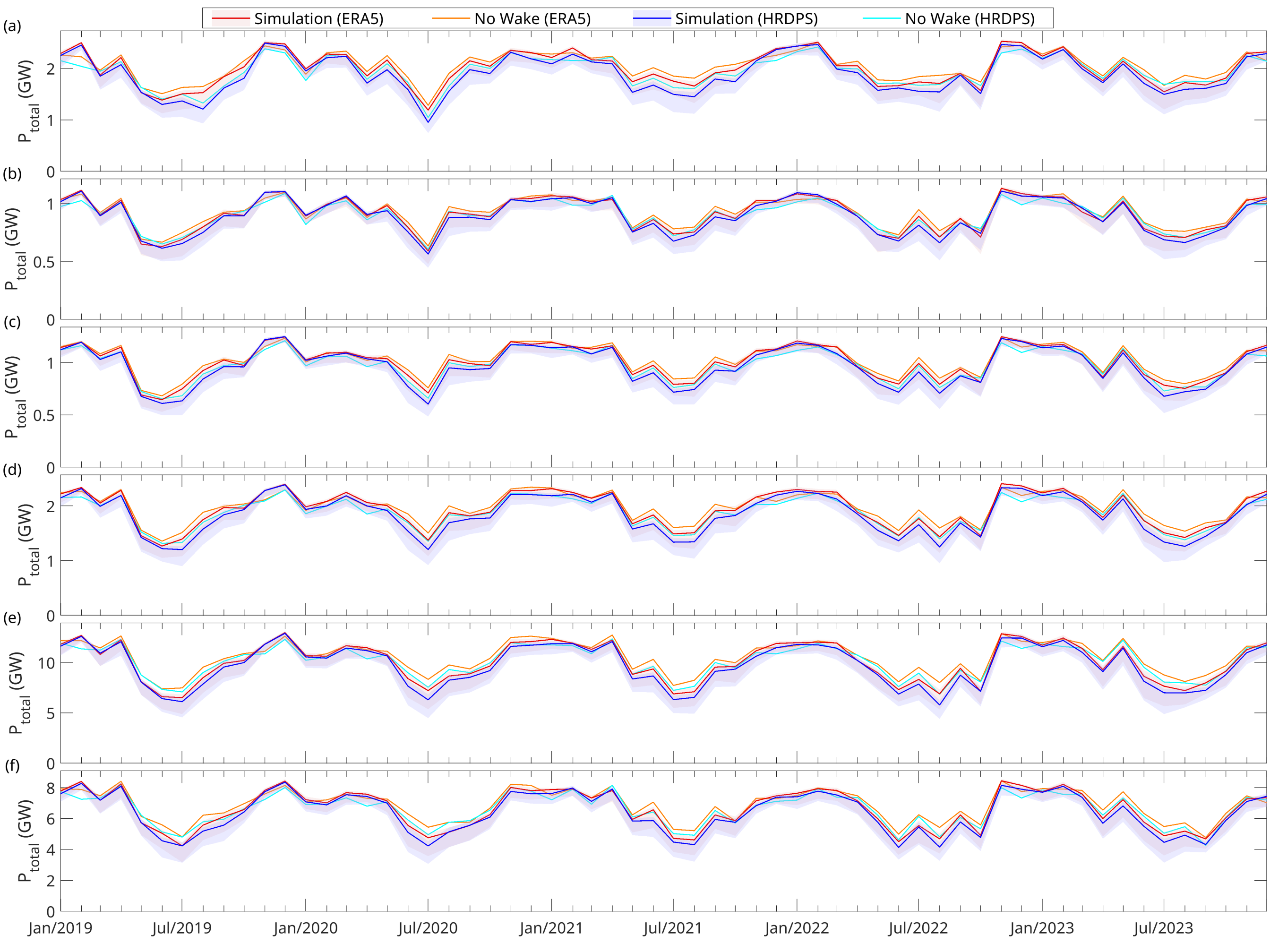

Figure 15. Same simulations described in Figure 13 and Table 7, except that the uncertainties are estimated to account for the wind direction estimation errors.

https://doi.org/10.5194/wes-2025-57
Preprint. Discussion started: 8 April 2025
© Author(s) 2025. CC BY 4.0 License.

WIND ENERGY SCIENCE DISCUSSIONS

Table 9. Seasonal mean values of total power production for the six potential future development areas (PFDAs) in winter (December to February) and summer (June to August) derived from the simulation results shown in Figure 15. Uncertainties are represented by the maximum deviations of the seasonal mean of the upper and lower bounds from the mean values.

PFDA	L/D	P_{total} (GW), ERA5		P_{total} (GW), HRDPS	
		Winter, Wake	Summer, Wake	Winter, Wake	Summer, Wake
Sydney Bight	9.6	2.4 ± 0.2	1.6 ± 0.3	2.3 ± 0.2	1.5 ± 0.3
Canso Bank	9.6	1.0 ± 0.1	0.8 ± 0.1	1.0 ± 0.1	0.7 ± 0.1
Eastern Shore	9.6	1.2 ± 0.1	0.8 ± 0.1	1.1 ± 0.1	0.8 ± 0.1
Middle Bank	9.6	2.3 ± 0.1	1.6 ± 0.3	2.2 ± 0.2	1.4 ± 0.3
Sable Island Bank	9.6	12.0 ± 0.9	7.7 ± 1.6	11.8 ± 0.9	7.1 ± 1.6
Emerald Bank	9.6	7.8 ± 0.5	5.1 ± 1.1	7.7 ± 0.6	4.8 ± 1.1

5.1 Wind Dataset Assessment

The wind datasets assessed in this study are widely used and have been evaluated in various regions worldwide (Fan et al., 2021; Fernandes et al., 2021; Li et al., 2010; Milbrandt et al., 2016). However, their performance can vary spatially, necessitating region-specific assessments. For wind farm development and design configurations, accuracy of modeled wind data is crucial for reliable energy potential estimates. On the Scotian Shelf, few studies have evaluated the applicability of various wind datasets to the region. This study provides a comprehensive assessment of wind speed and direction for the Scotian Shelf, providing a robust foundation for wind dataset selection in wind energy assessment.

The strong performance of ERA5 in the regional area of the Scotian Shelf aligned with previous studies for other regions, both inland and offshore (Fan et al., 2021; Murcia et al., 2022). These studies consistently found that ERA5 exhibited lower biases and mean absolute errors, along with higher correlations compared to other wind datasets. The overall robust performance of ERA5 was likely attributed to its advanced data assimilation techniques (Hersbach et al., 2020). In offshore regions, in particular, ERA5 has proven to be highly reliable (Gualtieri, 2021). Even when compared to a high-resolution regional Weather Research & Forecasting (WRF) Model, which employed nested grids with resolution ranging from 18 km to 2 km, ERA5 (31 km resolution) had demonstrated superior performance. Gualtieri (2021) reported that ERA5 achieved lower RMSE and bias, along with a higher correlation coefficient, when validated against observations from an offshore mast in the North Sea. This advantage can be attributed to the relatively homogeneous wind conditions in offshore regions, where high-resolution models do not provide a notable improvement over ERA5. However, in nearshore areas, the results of this study revealed that HRDPS outperformed ERA5, consistent with the findings of Gualtieri (2021). The reduced performance of ERA5 in coastal transition areas can be attributed to significant differences in surface roughness and temperature, which introduced more complex flow dynamics (Gualtieri, 2021; Dörenkämper et al., 2015; Cañadillas et al., 2023; Djath et al., 2022). These findings highlighted the advantages of high-resolution numerical models, such as HRDPS (2.5 km), in improving the accuracy of wind speed and direction estimates in complex nearshore environments by better resolving small-scale dynamics.

https://doi.org/10.5194/wes-2025-57
Preprint. Discussion started: 8 April 2025
© Author(s) 2025. CC BY 4.0 License.

Electricity consumption fluctuates over time, exhibiting diurnal, weekly, and seasonal patterns. In Nova Scotia, energy consumption is typically higher during the colder months of December to February and lower during the warmer months of May to October (see: Figure A4). These variations underscore the importance of assessing wind datasets at different local times and across seasons, in order to better align wind energy production with electricity demand cycles. Results of this study revealed notable seasonal and diurnal variability in performance across the wind datasets. Errors in wind speed estimation were generally higher in the fall and winter months, aligning with periods of stronger and more variable winds. In contrast, the spring and summer months exhibited lower errors.

At some offshore sites that had wind observations from marine buoys, wind directions from all datasets consistently had discrepancies during certain periods. Such consistent discrepancies across all datasets were likely caused by an inaccurate measurement of wind direction measured at the marine buoy at some locations. Unlike wind speed, which is relatively easy to measure, measuring wind direction is more difficult. Multiple factors, such as buoy motion due to waves or a misalignment of buoy orientation relative to true north, can cause error in wind direction measurements from such platforms (Malačič, 2019; Schlundt et al., 2020).

Beyond wind energy applications, the findings have broader implications for regional ocean modeling, where wind datasets serve as key surface boundary conditions. For large-scale ocean models of the Scotian Shelf, both ERA5 and HRDPS are viable wind datasets to use, while HRDPS is preferable for coastal modeling due to its natively finer resolution and improved representation of nearshore wind patterns.

5.2 Power Production Simulation

Wind energy estimates from wind speed using theoretical formulas often omit energy losses associated with turbine wakes (Nicholson, 2023; Wang et al., 2022). In reality, turbine wakes can significantly reduce total wind farm power output, with downstream effects extending to turbines located further along the flow field. These wake effects thus are key considerations when balancing energy production and overall wind farm efficiency, as the spacing between turbines and the positioning within the wind frame impact the effectiveness of the entire operation.

Simulations in this study emphasized the trade-off between potential energy production and turbine density. In this case, increased density amplified wake losses, which reduced overall efficiency. In contrast, greater turbine spacing decreased wake interactions that enhanced power output per turbine, but reduced the total energy yield due to fewer turbines occupying a given area.

The empirical piecewise function derived in this study provided valuable insights into the trade-off between energy generation efficiency and total power production, offering a quantitative framework for optimizing wind farm layouts. This two-regime function was characterized by a critical transition point, x_{t}, that defined the normalized turbine spacing beyond which wake effects became minimal. For smaller turbine spacings ($L/D < x_{\mathrm{t}}$), the function followed a Weibull-like function form, reaching its maximum at $L/D = x_{\mathrm{m}}$. Below this threshold, total power production declined due to intensified wake interactions. This suggested that normalized turbine spacings smaller than x_{m} should be avoided, as both total power output and wake efficiency decreased. For larger turbine spacings ($L/D > x_{\mathrm{t}}$), wake effects were minimal, leading to improved wake efficiency.

Winter wind conditions with higher wind speeds generally favored smaller turbine spacings. This was because the thrust coefficient (C_t) decreased at higher wind speeds, resulting in less significant wakes and faster wake recovery, which allowed turbines to be placed closer together without substantial efficiency losses. Consequently, the values of x_t and x_m were typically smaller in winter than in summer. For most PFDAs, achieving optimal wake efficiency in summer required the normalized turbine spacings within the range of 7.1 to 7.8. Meanwhile, maximizing total power production can be achieved by selecting a normalized turbine spacing corresponding to the mean value of x_m of both seasons, which ranged from 3.3 to 4.5.

Wake losses proved to be significant in the simulations, with values ranging from 17% to 26% in winter and 40% to 55% in summer in the dense turbine layout scenario. Power losses decreased as turbine spacing increased. In the scenario where turbine spacing was set to 9.6 D, the power losses became negligible in winter and were less than 12% in summer. The wake losses in the dense turbine layout scenario were generally higher than the 10% to 25% range reported in other studies on medium-sized offshore wind farms (Barthelmie et al., 2009, 2010; Niayifar and Porté-Agel, 2015; Simisiroglou et al., 2019; Wu and Porté-Agel, 2015). This discrepancy can be attributed to multiple factors, such as turbine models, spacings, and wind farm sizes. In the dense turbine layout scenario presented, turbine spacings that ranged from 3.3 to 4.5 were smaller than those in the aforementioned studies, which contributed to higher wake losses simulated in this study. Last, the findings presented in this study were in line with results of simulations for larger offshore wind farms reported by Pryor et al. (2021), who reported an overall wake loss of 35.3%. This value falls between the results for the dense turbine layout scenario in winter and summer within this study.

Uncertainties in total power output were also assessed based on discrepancies in both wind speed and wind direction between wind datasets and observations. To quantify these uncertainties, wind speed and wind direction time series were perturbed separately, where the dataset-specific RMSE was used to define the error bounds. This approach provided clear illustration of how wind speed and wind direction errors propagated into power estimations. Notably, in the dense layout scenario, errors in wind direction had an impact on power production that was just as significant as errors in wind speed. This result underscores the importance of wind direction accuracy in estimating power production, as deviations can alter wind turbine wake interactions and influence overall energy generation.

Limitations of perturbing wind speed or direction time series should be acknowledged. Perturbing wind speed involved simply adding or subtracting RMSE, while perturbing wind direction employed 10 evenly spaced values within the positive and negative RMSE bounds. Neither method accounted for the probability distribution of their respective errors; particularly, when the monthly wind speed or direction bias largely deviated from zero. As a result, this method may overestimate or underestimate the upper and lower bounds of the uncertainties. A more sophisticated approach, that could address this issue, would involve probabilistic uncertainty modeling, such as Monte Carlo simulations (Singh and Taylor, 2018; Liu et al., 2023) that provides a more rigorous representation of how wind speed or direction error distributions impact power estimations. However, compared to the Monte Carlo method, the approach used in this study was computationally efficient, making it a more practical choice for large-scale wind farm assessments.

Many studies that have simulated offshore wind farms have focused on annual or long-term mean energy production or capacity factors (Pryor et al., 2021; Simisiroglou et al., 2019; Wu and Porté-Agel, 2015), where the wind inputs consisted

https://doi.org/10.5194/wes-2025-57
Preprint. Discussion started: 8 April 2025
© Author(s) 2025. CC BY 4.0 License.

of several combinations of constant wind speeds and directions derived from historical wind statistics. However, temporal variation of power production has received comparatively less research focus (Wang et al., 2022). This study helps address this gap by analyzing the monthly time series of power production across PDFAs on the Scotian Shelf. Seasonal variations were pronounced, with summer production in the dense turbine layout being 44% to 55% lower than in winter. In the less dense 9.6 D layout, reductions in summer power production ranged from 28% to 36% compared to winter. Despite these fluctuations, seasonal wind power generation patterns closely aligned with seasonal variation in Nova Scotia electricity demand, which peaks in the winter and declines in the summer. This alignment suggests that offshore wind has the potential to complement Nova Scotia's seasonal electricity demand, reinforcing the importance of incorporating temporal variability into wind energy assessments.

6 Conclusion

This research study is the first comprehensive assessment of wind speed and direction data from four widely used wind datasets—ERA5, CFSv2, NARR and HRDPS—across the Scotian Shelf, which is a region with world-class wind energy potential. The analyses highlighted spatial and temporal variability in dataset performance, with HRDPS emerged as the most accurate dataset for nearshore wind conditions, while ERA5 proved the most reliable for broader offshore areas. Seasonal and diurnal variations further underscored the need for careful dataset selection when modelling wind energy potential.

The PFDA simulations using PyWake demonstrated the significant impact of wake interactions and turbine spacing on energy production. The results highlighted trade-offs in maximizing total power output and minimizing wake-induced losses. For most PFDAs, achieving effective wake efficiency year-round required turbine spacing of 7.1–7.8 D, whereas maximizing total power production was best achieved with a denser layout of 3.3–4.5 D. Seasonal variations further influenced wake dynamics, reinforcing the importance of considering temporal wind variability.

Overall, the research findings provided valuable insights for offshore wind development in Nova Scotia, emphasizing the need for accurate wind resource assessment and strategic turbine layout. Through integration of high-resolution wind datasets and accounting for seasonal and wake effects, wind farm design on the Scotian Shelf can be optimized for energy production and long-term efficiency.

Data availability. The data generated in this study is available upon reasonable request.

https://doi.org/10.5194/wes-2025-57
Preprint. Discussion started: 8 April 2025
© Author(s) 2025. CC BY 4.0 License.

735 **Appendix A: Appendix**

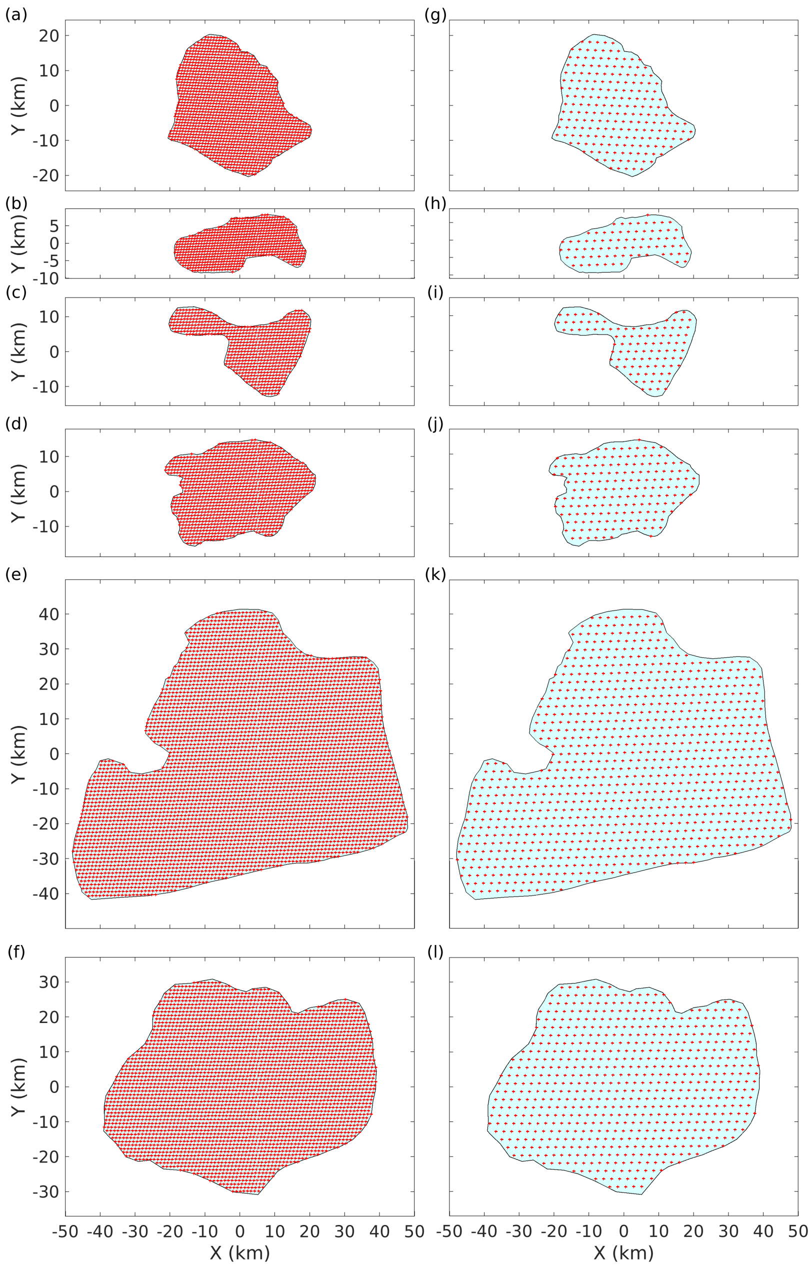

Figure A1. Diagrams of the layouts of wind turbines for the six potential future development areas (PFDAs): (a, g) Sydney Bight, (b, h) Canso Bank, (c, i) Eastern Shore, (d, j) Middle Bank, (e, k) Sable Island Bank, and (f, l) Emerald Bank. The normalized turbine spacings (L/D) for the left panels are 3.5, 3.3, 3.7, 3.8, 4.5 and 4.4, respectively, and 9.6 for all right panels. Refer to Figure 1 for location of PFDAs on the Scotian Shelf.

https://doi.org/10.5194/wes-2025-57
Preprint. Discussion started: 8 April 2025
© Author(s) 2025. CC BY 4.0 License.
Open Access
WIND ENERGY SCIENCE
DISCUSSIONS

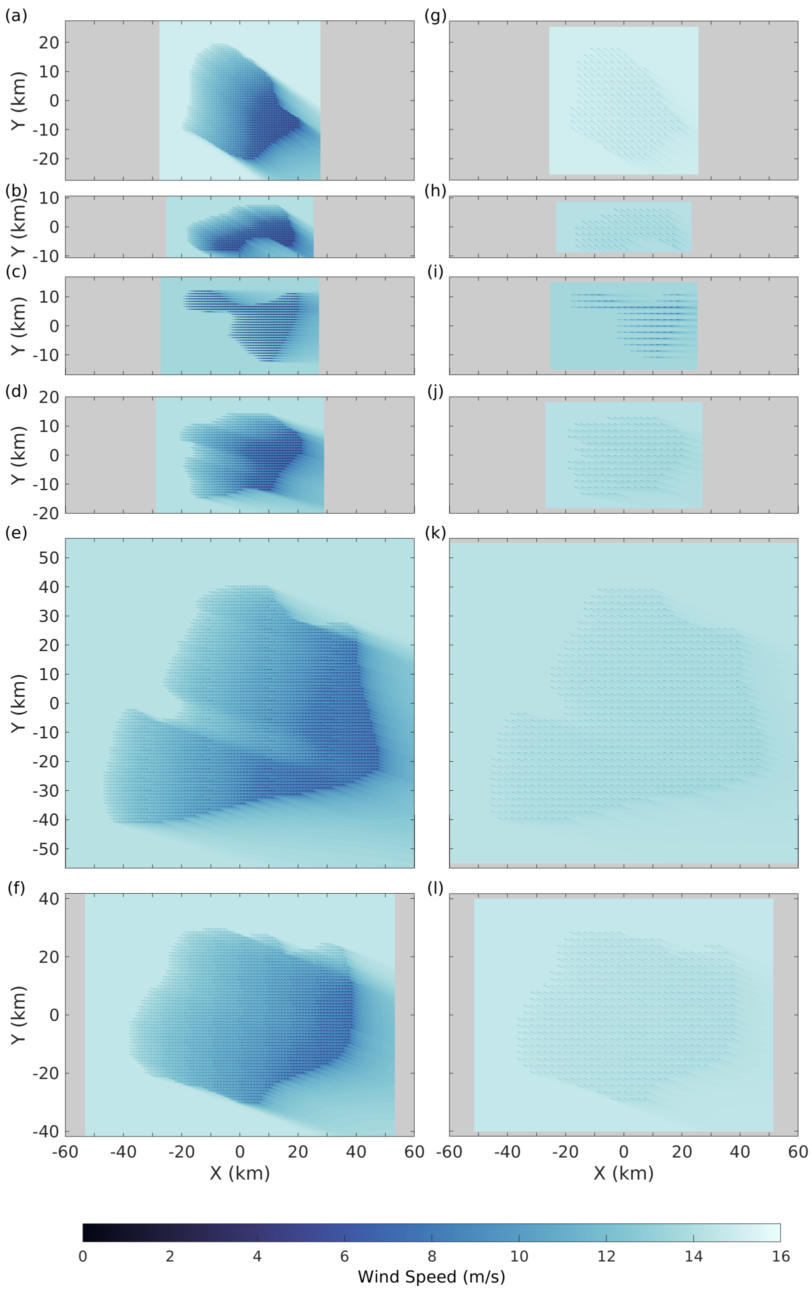

Figure A2. Flow maps of wind speed at the hub height of 150 m and wake effects simulated using PyWake for the six potential future development areas (PFDAs): (a, g) Sydney Bight, (b, h) Canso Bank, (c, i) Eastern Shore, (d, j) Middle Bank, (e, k) Sable Island Bank, and (f, l) Emerald Bank during winter, with the layouts same as in Figure A1. The wind dataset used was ERA5. Refer to Figure 1 for location of PDFAs on the Scotian Shelf.

https://doi.org/10.5194/wes-2025-57
Preprint. Discussion started: 8 April 2025
© Author(s) 2025. CC BY 4.0 License.

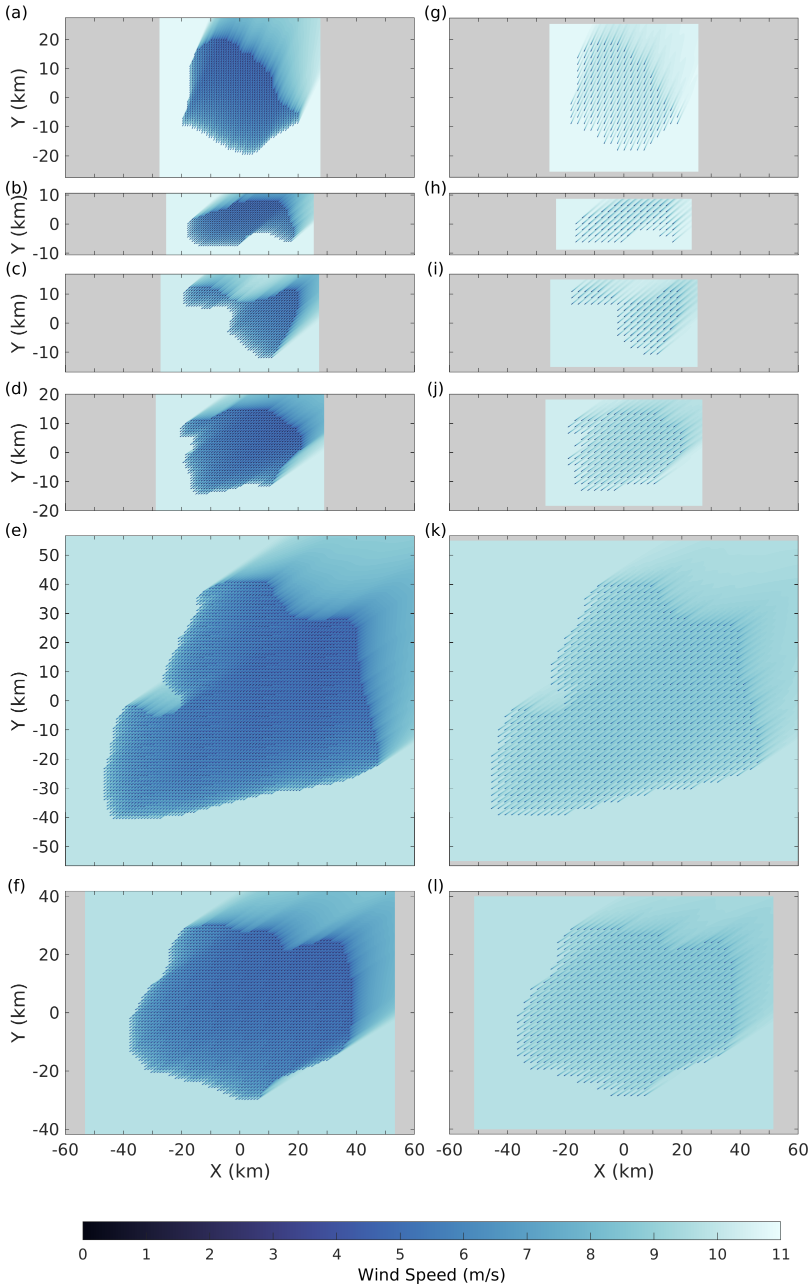

Figure A3. Flow maps of wind speed at the hub height of 150 m and wake effects simulated using PyWake for the six potential future development areas (PFDAs): (a, g) Sydney Bight, (b, h) Canso Bank, (c, i) Eastern Shore, (d, j) Middle Bank, (e, k) Sable Island Bank, and (f, l) Emerald Bank during summer, with the layouts same as in Figure A1. The wind dataset used was ERA5. Refer to Figure 1 for location of PDFAs on the Scotian Shelf.

https://doi.org/10.5194/wes-2025-57
Preprint. Discussion started: 8 April 2025
© Author(s) 2025. CC BY 4.0 License.

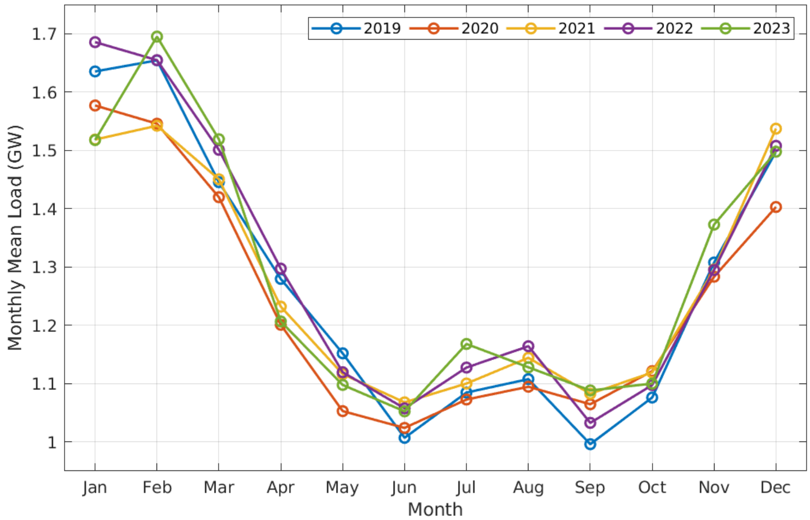

Figure A4. Monthly mean load for Nova Scotia, Canada, in 2019–2023. Data sourced from the website of Nova Scotia Power: https://www.nspower.ca/oasis/monthly-reports/hourly-total-net-nova-scotia-load.

Author contributions. Yongxing Ma: Data Curation, Methodology, Software, Formal Analysis, Visualization, Writing – Original Draft, Writing – Review & Editing. Jinshan Xu: Writing – Review & Editing. Yongsheng Wu: Conceptualization, Methodology, Funding Acquisition, Project Administration, Supervision, Writing – Review & Editing. Michael Z. Li: Writing – Review & Editing. Ryan Stanley: Writing – Review & Editing. Brent Law: Writing – Review & Editing. Marc Skinner: Writing – Review & Editing. All authors have reviewed and approved the final manuscript.

Competing interests. The authors declare that they have no conflict of interest.

Acknowledgements. This research study was funded under the Fisheries and Oceans Canada (DFO) Competitive Science Research Fund (CSRF, fund number 2024-25-04-01) awarded to Y. Wu. The authors thank A. Cogswell for his invaluable support and advice throughout proposal preparation and submission. The authors also thank K. Curran and E. Nagel for their meaningful review and comments on an early version of the manuscript.

References

Aegir Insights ApS: Value Mapping Nova Scotia's Offshore Wind Resources, Tech. rep., https://netzeroatlantic.ca/sites/default/files/2023-04/Value%20Mapping%20Nova%20Scotia%20Offshore%20Wind%20Resources.pdf, 2023.

Barthelmie, R. J., Hansen, K., Frandsen, S. T., Rathmann, O., Schepers, J. G., Schlez, W., Phillips, J., Rados, K., Zervos, A., Politis, E. S., and Chaviaropoulos, P. K.: Modelling and Measuring Flow and Wind Turbine Wakes in Large Wind Farms Offshore, Wind Energy, 12, 431–444, https://doi.org/10.1002/we.348, 2009.

Barthelmie, R. J., Pryor, S. C., Frandsen, S. T., Hansen, K. S., Schepers, J. G., Rados, K., Schlez, W., Neubert, A., Jensen, L. E., and Neckelmann, S.: Quantifying the Impact of Wind Turbine Wakes on Power Output at Offshore Wind Farms, Journal of Atmospheric and Oceanic Technology, 27, 1302–1317, https://doi.org/10.1175/2010JTECHA1398.1, 2010.

Bastankhah, M. and Porté-Agel, F.: A New Analytical Model for Wind-Turbine Wakes, Renewable Energy, 70, 116–123, https://doi.org/10.1016/j.renene.2014.01.002, 2014.

Berens, P.: **CircStat** : A *MATLAB* Toolbox for Circular Statistics, Journal of Statistical Software, 31, https://doi.org/10.18637/jss.v031.i10, 2009.

Bosch, J., Staffell, I., and Hawkes, A. D.: Global Levelised Cost of Electricity from Offshore Wind, Energy, 189, 116 357, https://doi.org/10.1016/j.energy.2019.116357, 2019.

Calaf, M., Meneveau, C., and Meyers, J.: Large Eddy Simulation Study of Fully Developed Wind-Turbine Array Boundary Layers, Physics of Fluids, 22, 015 110, https://doi.org/10.1063/1.3291077, 2010.

Canada, N. R.: Powering Canada's Future: A Clean Electricity Strategy, https://natural-resources.canada.ca/energy-sources/powering-canada-s-future-clean-electricity-strategy, accessed: 2025-03-26, n.d.

Canada Energy Regulator: Canada's Energy Future 2023: Energy Supply and Demand Projections to 2050, Tech. rep., Canada Energy Regulator, 2023.

Cañadillas, B., Wang, S., Ahlert, Y., Djath, B., Barekzai, M., Foreman, R., and Lampert, A.: Coastal Horizontal Wind Speed Gradients in the North Sea Based on Observations and ERA5 Reanalysis Data, Meteorologische Zeitschrift, 32, 207–228, https://doi.org/10.1127/metz/2022/1166, 2023.

Chamorro, L. P. and Porté-Agel, F.: Effects of Thermal Stability and Incoming Boundary-Layer Flow Characteristics on Wind-Turbine Wakes: A Wind-Tunnel Study, Boundary-Layer Meteorology, 136, 515–533, https://doi.org/10.1007/s10546-010-9512-1, 2010.

Committee for the Regional Assessment of Offshore Wind Development in Nova Scotia: Regional Assessment of Offshore Wind Development in Nova Scotia: Interim Report, Tech. rep., https://iaac-aeic.gc.ca/050/documents/p83514/156045E.pdf, 2024.

Djath, B., Schulz-Stellenfleth, J., and Cañadillas, B.: Study of Coastal Effects Relevant for Offshore Wind Energy Using Spaceborne Synthetic Aperture Radar (SAR), Remote Sensing, 14, 1688, https://doi.org/10.3390/rs14071688, 2022.

Dörenkämper, M., Optis, M., Monahan, A., and Steinfeld, G.: On the Offshore Advection of Boundary-Layer Structures and the Influence on Offshore Wind Conditions, Boundary-Layer Meteorology, 155, 459–482, https://doi.org/10.1007/s10546-015-0008-x, 2015.

Fan, W., Liu, Y., Chappell, A., Dong, L., Xu, R., Ekström, M., Fu, T.-M., and Zeng, Z.: Evaluation of Global Reanalysis Land Surface Wind Speed Trends to Support Wind Energy Development Using In Situ Observations, Journal of Applied Meteorology and Climatology, 60, 33–50, https://doi.org/10.1175/JAMC-D-20-0037.1, 2021.

https://doi.org/10.5194/wes-2025-57
Preprint. Discussion started: 8 April 2025
© Author(s) 2025. CC BY 4.0 License.

WIND ENERGY SCIENCE DISCUSSIONS

Fernandes, I. G., Pimenta, F. M., Saavedra, O. R., and Silva, A. R.: Offshore Validation of ERA5 Reanalysis with Hub Height Wind Observations of Brazil, in: 2021 IEEE PES Innovative Smart Grid Technologies Conference - Latin America (ISGT Latin America), pp. 1–5, IEEE, Lima, Peru, ISBN 978-1-6654-4421-7, https://doi.org/10.1109/ISGTLatinAmerica52371.2021.9542993, 2021.

Fischereit, J., Schaldemose Hansen, K., Larsén, X. G., Van Der Laan, M. P., Réthoré, P.-E., and Murcia Leon, J. P.: Comparing and Validating Intra-Farm and Farm-to-Farm Wakes across Different Mesoscale and High-Resolution Wake Models, Wind Energy Science, 7, 1069–1091, https://doi.org/10.5194/wes-7-1069-2022, 2022.

Frandsen, S.: On the Wind Speed Reduction in the Center of Large Clusters of Wind Turbines, Journal of Wind Engineering and Industrial Aerodynamics, 39, 251–265, https://doi.org/10.1016/0167-6105(92)90551-K, 1992.

Gaertner, E., Rinker, J., Sethuraman, L., Zahle, F., Anderson, B., Barter, G., Abbas, N., Meng, F., Bortolotti, P., Skrzypinski, W., Scott, G., Feil, R., Bredmose, H., Dykes, K., Shields, M., Allen, C., and Viselli, A.: Definition of the IEA 15-Megawatt Offshore Reference Wind, Golden, CO: National Renewable Energy Laboratory, 2020.

Gaumond, M., Réthoré, P.-E., Ott, S., Peña, A., Bechmann, A., and Hansen, K. S.: Evaluation of the Wind Direction Uncertainty and Its Impact on Wake Modeling at the Horns Rev Offshore Wind Farm, Wind Energy, 17, 1169–1178, https://doi.org/10.1002/we.1625, 2014.

Government of Nova Scotia: Nova Scotia Offshore Wind Roadmap: Module 1, Tech. rep., Government of Nova Scotia, Nova Scotia, Canada, https://novascotia.ca/offshore-wind/docs/offshore-wind-roadmap-module-1.pdf, 2023.

Gualtieri, G.: Reliability of ERA5 Reanalysis Data for Wind Resource Assessment: A Comparison against Tall Towers, Energies, 14, 4169, https://doi.org/10.3390/en14144169, 2021.

Hansen, K. S., Barthelmie, R. J., Jensen, L. E., and Sommer, A.: The Impact of Turbulence Intensity and Atmospheric Stability on Power Deficits Due to Wind Turbine Wakes at Horns Rev Wind Farm, Wind Energy, 15, 183–196, https://doi.org/10.1002/we.512, 2012.

Hersbach, H., Bell, B., Berrisford, P., Hirahara, S., Horányi, A., Muñoz-Sabater, J., Nicolas, J., Peubey, C., Radu, R., Schepers, D., Simmons, A., Soci, C., Abdalla, S., Abellan, X., Balsamo, G., Bechtold, P., Biavati, G., Bidlot, J., Bonavita, M., De Chiara, G., Dahlgren, P., Dee, D., Diamantakis, M., Dragani, R., Flemming, J., Forbes, R., Fuentes, M., Geer, A., Haimberger, L., Healy, S., Hogan, R. J., Hólm, E., Janisková, M., Keeley, S., Laloyaux, P., Lopez, P., Lupu, C., Radnoti, G., De Rosnay, P., Rozum, I., Vamborg, F., Villaume, S., and Thépaut, J.-N.: The ERA5 Global Reanalysis, Quarterly Journal of the Royal Meteorological Society, 146, 1999–2049, https://doi.org/10.1002/qj.3803, 2020.

Hersbach, H., Bell, B., Berrisford, P., Biavati, G., Horányi, A., Muñoz Sabater, J., Nicolas, J., Peubey, C., Radu, R., Rozum, I., Schepers, D., Simmons, A., Soci, C., Dee, D., and Thépaut, J.-N.: ERA5 Hourly Data on Single Levels from 1940 to Present, https://doi.org/10.24381/cds.adbb2d47, 2023.

Holt, E. and Wang, J.: Trends in Wind Speed at Wind Turbine Height of 80 m over the Contiguous United States Using the North American Regional Reanalysis (NARR), Journal of Applied Meteorology and Climatology, 51, 2188–2202, https://doi.org/10.1175/JAMC-D-11-0205.1, 2012.

Hou, P., Zhu, J., Ma, K., Yang, G., Hu, W., and Chen, Z.: A Review of Offshore Wind Farm Layout Optimization and Electrical System Design Methods, Journal of Modern Power Systems and Clean Energy, 7, 975–986, https://doi.org/10.1007/s40565-019-0550-5, 2019.

Jensen, N. O.: A Note on Wind Generator Interaction, no. 2411 in Risø-M, Risø National Laboratory, ISBN 87-550-0971-9, 1983.

Kardakaris, K., Boufidi, I., and Soukissian, T.: Offshore Wind and Wave Energy Complementarity in the Greek Seas Based on ERA5 Data, Atmosphere, 12, 1360, https://doi.org/10.3390/atmos12101360, 2021.

Kilpatrick, R. J., Wakim, C., and Caesar, G.: Preliminary Considerations Analysis of Offshore Wind Energy in Atlantic Canada, Tech. rep., https://doi.org/10.4095/331855, 2023.

https://doi.org/10.5194/wes-2025-57
Preprint. Discussion started: 8 April 2025
© Author(s) 2025. CC BY 4.0 License.

Li, X., Zhong, S., Bian, X., and Heilman, W. E.: Climate and Climate Variability of the Wind Power Resources in the Great Lakes Region of the United States, Journal of Geophysical Research: Atmospheres, 115, 2009JD013 415, https://doi.org/10.1029/2009JD013415, 2010.

Liu, R., Peng, L., Huang, G., Zhou, X., Yang, Q., and Cai, J.: A Monte Carlo Simulation Method for Probabilistic Evaluation of Annual Energy Production of Wind Farm Considering Wind Flow Model and Wake Effect, Energy Conversion and Management, 292, 117 355, https://doi.org/10.1016/j.enconman.2023.117355, 2023.

Malačič, V.: Wind Direction Measurements on Moored Coastal Buoys, Journal of Atmospheric and Oceanic Technology, 36, 1401–1418, https://doi.org/10.1175/JTECH-D-18-0171.1, 2019.

McCoy, A., Musial, W., Hammond, R., Hernando, D. M., Duffy, P., Beiter, P., Pérez, P., Baranowski, R., Reber, G., and Spitsen, P.: Offshore Wind Market Report: 2024 Edition, Tech. Rep. NREL/TP-5000-90525, Golden, CO: National Renewable Energy Laboratory, 2024.

Mesinger, F., DiMego, G., Kalnay, E., Mitchell, K., Shafran, P. C., Ebisuzaki, W., Jović, D., Woollen, J., Rogers, E., Berbery, E. H., Ek, M. B., Fan, Y., Grumbine, R., Higgins, W., Li, H., Lin, Y., Manikin, G., Parrish, D., and Shi, W.: North American Regional Reanalysis, Bulletin of the American Meteorological Society, 87, 343–360, https://doi.org/10.1175/BAMS-87-3-343, 2006.

Milbrandt, J. A., Bélair, S., Faucher, M., Vallée, M., Carrera, M. L., and Glazer, A.: The Pan-Canadian High Resolution (2.5 Km) Deterministic Prediction System, Weather and Forecasting, 31, 1791–1816, https://doi.org/10.1175/WAF-D-16-0035.1, 2016.

Moore-Maley, B. and Allen, S. E.: Wind-Driven Upwelling and Surface Nutrient Delivery in a Semi-Enclosed Coastal Sea, Ocean Science, 18, 143–167, https://doi.org/10.5194/os-18-143-2022, 2022.

Mulas Hernando, D., Musial, W., Duffy, P., and Shields, M.: Capacity Density Considerations for Offshore Wind Plants in the United States, Tech. Rep. NREL/TP–5000-86933, 2274825, MainId:87708, https://doi.org/10.2172/2274825, 2023.

Murcia, J. P., Koivisto, M. J., Luzia, G., Olsen, B. T., Hahmann, A. N., Sørensen, P. E., and Als, M.: Validation of European-scale Simulated Wind Speed and Wind Generation Time Series, Applied Energy, 305, 117 794, https://doi.org/10.1016/j.apenergy.2021.117794, 2022.

National Centers for Environmental Prediction, National Weather Service, NOAA, U.S. Department of Commerce: NCEP North American Regional Reanalysis (NARR), https://rda.ucar.edu/datasets/dsd608000/, 2005.

Niayifar, A. and Porté-Agel, F.: A New Analytical Model for Wind Farm Power Prediction, Journal of Physics: Conference Series, 625, 012 039, https://doi.org/10.1088/1742-6596/625/1/012039, 2015.

Nicholson, P.: Catching the Wind: How Atlantic Canada Can Become an Energy Superpower, Atlantic Momentum Series, Public Policy Forum, Ottawa, ON, Canada, ISBN 978-1-77452-136-6, 2023.

Pedersen, M. M., Forsting, A. M., van der Laan, P., Riva, R., Alcayaga Romàn, L. A., Criado Risco, J., Friis-Møller, M., Quick, J., Schøler Christiansen, J. P., Valotta Rodrigues, R., Olsen, B. T., and Réthoré, P.-E.: PyWake 2.5.0: An Open-Source Wind Farm Simulation Tool, DTU Wind, Technical University of Denmark, 2023.

Pryor, S. C., Barthelmie, R. J., and Shepherd, T. J.: Wind Power Production from Very Large Offshore Wind Farms, Joule, 5, 2663–2686, https://doi.org/10.1016/j.joule.2021.09.002, 2021.

PyWake development team: Automated validation report for PyWake, Tech. rep., DTU Wind Energy, n.d.

Quick, J., Mouradi, R.-S., Devesse, K., Mathieu, A., Paul Van Der Laan, M., Murcia Leon, J. P., and Schulte, J.: Verification and Validation of Wind Farm Flow Models, Journal of Physics: Conference Series, 2767, 092 074, https://doi.org/10.1088/1742-6596/2767/9/092074, 2024.

Rezaei, F., Contestabile, P., Vicinanza, D., and Azzellino, A.: Towards Understanding Environmental and Cumulative Impacts of Floating Wind Farms: Lessons Learned from the Fixed-Bottom Offshore Wind Farms, Ocean & Coastal Management, 243, 106 772, https://doi.org/10.1016/j.ocecoaman.2023.106772, 2023.

© Author(s) 2025. CC BY 4.0 License.

Saha, S., Moorthi, S., Wu, X., Wang, J., Nadiga, S., Tripp, P., Behringer, D., Hou, Y.-T., Chuang, H.-y., Iredell, M., Ek, M., Meng, J., Yang, R., Mendez, M. P., van den Dool, H., Zhang, Q., Wang, W., Chen, M., and Becker, E.: NCEP Climate Forecast System Version 2 (CFSv2) Selected Hourly Time-Series Products, 2011.

Saha, S., Moorthi, S., Wu, X., Wang, J., Nadiga, S., Tripp, P., Behringer, D., Hou, Y.-T., Chuang, H.-y., Iredell, M., Ek, M., Meng, J., Yang, R., Mendez, M. P., Van Den Dool, H., Zhang, Q., Wang, W., Chen, M., and Becker, E.: The NCEP Climate Forecast System Version 2, Journal of Climate, 27, 2185–2208, https://doi.org/10.1175/JCLI-D-12-00823.1, 2014.

Schlundt, M., Farrar, J. T., Bigorre, S. P., Plueddemann, A. J., and Weller, R. A.: Accuracy of Wind Observations from Open-Ocean Buoys: Correction for Flow Distortion, Journal of Atmospheric and Oceanic Technology, 37, 687–703, https://doi.org/10.1175/JTECH-D-19-0132.1, 2020.

Simisiroglou, N., Polatidis, H., and Ivanell, S.: Wind Farm Power Production Assessment: Introduction of a New Actuator Disc Method and Comparison with Existing Models in the Context of a Case Study, Applied Sciences, 9, 431, https://doi.org/10.3390/app9030431, 2019.

Singh, S. and Taylor, J. H.: Uncertainty Estimation in Wind Power Forecasts Using Monte Carlo Simulations, in: 2018 IEEE Canadian Conference on Electrical & Computer Engineering (CCECE), pp. 1–6, IEEE, Quebec, QC, Canada, ISBN 978-1-5386-2410-4, https://doi.org/10.1109/CCECE.2018.8447846, 2018.

Stevens, R. J. A. M.: Dependence of Optimal Wind Turbine Spacing on Wind Farm Length: Stevens, Dependence of Optimal Wind-Turbine Spacing on Windfarm Length, Wind Energy, 19, 651–663, https://doi.org/10.1002/we.1857, 2016.

Stevens, R. J. A. M., Hobbs, B. F., Ramos, A., and Meneveau, C.: Combining Economic and Fluid Dynamic Models to Determine the Optimal Spacing in Very Large Wind Farms, Wind Energy, 20, 465–477, https://doi.org/10.1002/we.2016, 2017.

Stieren, A., Gadde, S. N., and Stevens, R. J.: Modeling Dynamic Wind Direction Changes in Large Eddy Simulations of Wind Farms, Renewable Energy, 170, 1342–1352, https://doi.org/10.1016/j.renene.2021.02.018, 2021.

Tetra Tech Inc.: Empire Offshore Wind: Empire Wind Project (EW 1 and EW 2) Construction and Operations Plan, Tech. rep., Tetra Tech Inc., 2022.

Tian, Q., Huang, G., Hu, K., and Niyogi, D.: Observed and Global Climate Model Based Changes in Wind Power Potential over the Northern Hemisphere during 1979–2016, Energy, 167, 1224–1235, https://doi.org/10.1016/j.energy.2018.11.027, 2019.

Troldborg, N., Sorensen, J. N., and Mikkelsen, R.: Numerical Simulations of Wake Characteristics of a Wind Turbine in Uniform Inflow, Wind Energy, 13, 86–99, https://doi.org/10.1002/we.345, 2010.

Wang, J., Hu, J., and Ma, K.: Wind Speed Probability Distribution Estimation and Wind Energy Assessment, Renewable and Sustainable Energy Reviews, 60, 881–899, https://doi.org/10.1016/j.rser.2016.01.057, 2016.

Wang, Y.-H., Walter, R. K., White, C., Kehrli, M. D., Hamilton, S. F., Soper, P. H., and Ruttenberg, B. I.: Spatial and Temporal Variation of Offshore Wind Power and Its Value along the Central California Coast, Environmental Research Communications, 1, 121 001, https://doi.org/10.1088/2515-7620/ab4ee1, 2019.

Wang, Y.-H., Walter, R. K., White, C., Kehrli, M. D., and Ruttenberg, B.: Scenarios for Offshore Wind Power Production for Central California Call Areas, Wind Energy, 25, 23–33, https://doi.org/10.1002/we.2646, 2022.

World Forum Offshore Wind: Global Offshore Wind Report 2023, Tech. rep., World Forum Offshore Wind (WFO), Hamburg, Taipei, New York, Tokyo, 2024.

Wu, Y.-T. and Porté-Agel, F.: Modeling Turbine Wakes and Power Losses within a Wind Farm Using LES: An Application to the Horns Rev Offshore Wind Farm, Renewable Energy, 75, 945–955, https://doi.org/10.1016/j.renene.2014.06.019, 2015.